Caenagnathids of the Hell Creek: A new specimen and volumetric mass estimation of *Anzu wyliei*

By
©2021
Kyle Atkins-Weltman
B.Sc. University of Kansas, 2018

Submitted to the graduate degree program in Ecology and Evolutionary Biology and the Graduate Faculty of the University of Kansas in partial fulfillment of the requirements for the degree of Master of Science.

_____

Chair: Dr. Bruce Lieberman

_____

Co-Chair: Dr. David Burnham

_____

Dr. Richard Glor

_____

Dr. Lena Hileman

_____

Dr. Eric Snively

Date Defended: 12 April 2021

The thesis committee for Kyle Atkins-Weltman certifies that this is the approved version of the following thesis:

Caenagnathids of the Hell Creek: A new specimen and volumetric mass estimation of *Anzu wyliei*

_____

Chair: Dr. Bruce Lieberman

_____

Co-chair: Dr. David Burnham

_____

Dr. Richard Glor

_____

Dr. Lena Hileman

_____

Dr. Eric Snively

Date Approved: 12 April 2021

Abstract

Caenagnathidae is a clade of derived oviraptorosaurian theropods that existed in both Asia and North America during the late Cretaceous, forming the sister clade to Oviraptoridae. While the oviraptorids are known from many well-preserved fossils including brooding specimens and with preserved feathers, the caenagnathid record is less spectacular, particularly from North America. Here, specimens of caenagnathids are rare and fragmentary. The largest North America caenagnathid, *Anzu wyliei,* from the end-Maastrichtian Hell Creek Formation, is the most complete caenagnathid from North America, and is the only one currently described from that time period. However, the question remains whether or not *Anzu wyliei* was the only caenagnathid of its time. Here, I describe a new, much smaller caenagnathid specimen from the Hell Creek Formation consisting of several hindlimb elements. A histological analysis was conducted to determine approximate age at the time of death and for comparison to the much larger *Anzu wyliei*. Based on several histological and osteological traits, I found that this new specimen was not a juvenile *Anzu wyliei*, but instead a subadult of a second, undescribed species of caenagnathid from the Hell Creek formation, more closely related to *Elmisaurus rarus* and *Citipes elegans* than to *A. wyliei*. The ability to accurately and reliably estimate body mass of extinct taxa is a vital tool for interpreting the physiology and even behavior of long-dead animals. For this reason, paleontologists have experimented with many possible methods of estimating the body mass of extinct animals, with varying degrees of success. These methods can be divided into two main categories: volumetric mass estimation, and extant scaling methods. Each has advantages and disadvantages, which is why, when possible, it is best to perform both, and compare the results to determine what is best within reason. Here I employ volumetric mass estimation (VME) to calculate an approximate body mass for previously described specimens of

Anzu wyliei from the Carnegie Museum of Natural History. I also use extant scaling methods to try to obtain a reliable mass estimate for this taxon. In addition, I present the first digital life restoration and convex hull of the dinosaur *Anzu wyliei* used for mass estimation purposes. I found that the volumetric mass estimation using my digital model was 216 - 280kg, which falls within the range predicted by extant scaling techniques, while the mass estimate using minimum convex hulls was below the predicted range, between 159 - 199kg. The VME method for *Anzu wyliei* strongly affirms the predictive utility of extant-based scaling. However, volumetric mass estimates are likely more precise because the models are based on comprehensive specimen anatomy rather than regressions of a phylogenetically comprehensive but disparate sample.

Acknowledgements

For facilitating specimen access as well as giving advice for transporting fossils, I thank both Matthew Lamanna and Amy Henrici. Nicolás Campione also deserves recognition for providing information and code for R-generated regressions of body mass from femoral circumference. For general comments and revisions on the project at multiple steps along the way, I would like to thank Nathan Van Vranken, Robert J. Gay, Heinrich Mallison, and of course all those on my advisory committee. For invaluable assistance with Caenagnathid characters, and for providing the beautiful time-calibrated phylogeny from the data I entered into the data matrix, I would like to thank Gregory Funston. For her generosity in creating the thin sections of bones and providing the histological analysis, Holly J. Woodward deserves immense gratitude. I also thank D.J. Pugh for his assistance in specimen photography, and Jackson Leibach for creating the specimen plates. I also extend my thanks to Lucy Roberts, who allowed me to use her scans of *Anzu wyliei* presacral vertebrae. I thank Evelyn Volmer who sculpted the missing skeletal elements and provided an articulated model of the skeleton. I also acknowledge Emma Schachner, who provided photographs of the axial skeleton of the CM *Anzu* specimens, which proved essential for manually sculpting elements that were not digitized. Scott Hartman's skeletal diagrams proved invaluable for sculpting the initial basis of the life restoration and informing basic articulation of the skeletal elements, and deserves acknowledgement for his work. Additionally, I thank Samuel Gutherz and Pat O'Connor for providing discussions of theropod air sac anatomy and indicating the proper placement and size of these structures within a digitized skeleton. Lastly but no less importantly, I would like to thank my fathers, John J. Weltman and James C. Atkins, for continuously providing their support and love, without which this project would not have been possible.

Table of Contents

Chapter 1

Osteological and Histological Assessment of a new Caenagnathid specimen from the Hell Creek Formation

ABSTRACT

Caenagnathidae is a clade of derived oviraptorosaurian theropods that existed in both Asia and North America during the Late Cretaceous, forming the sister clade to Oviraptoridae. While the oviraptorids are known from many well-preserved fossils including brooding specimens and those with preserved feathers, the caenagnathid record is less spectacular, particularly from North America. Here, specimens of caenagnathids are rare and fragmentary.. Here, I describe a new, much smaller caenagnathid specimen from the Hell Creek Formation consisting of several hindlimb elements, upon which I conducted histological analysis to determine approximate age at the time of death and for comparison to the [GRE1] much larger *Anzu wyliei*. Based on several histological and osteological traits, I foundthat this new specimen was not a juvenile *Anzu wyliei*, but instead a subadult of a second, undescribed species of caenagnathid from the Hell Creek formation, more closely related to *Elmisaurus rarus* and *Citipes elegans* than to *A. wyliei*.

INTRODUCTION

Oviraptorosauria is a clade of maniraptoran theropods with a distinctive craniomandibular anatomy that makes them immediately identifiable - all but the earliest members have edentulous beaks, and many possess crests of some form running along their skull [1]. The group is known from a number of well-preserved fossils, primarily from Asia, that have yielded insight into the biology, morphology, diversity, and evolutionary history of this peculiar group of theropods. The most recent research places their origins in the Barremian stage of the early Cretaceous, between 125-129 million years ago [2], and they persisted until the K-Pg extinction event. Oviraptorosaurs ranged in size from that of a chicken or turkey [3,4] to taxa posited to weigh over a tonne [5]. Though the earliest members of this group did retain teeth [3], this trait was entirely lost by Late Cretaceous forms. Spectacularly preserved fossils show that most oviraptorosaurs were covered in some form of feathery integument. Well-preserved bony fossils even show evidence of feathery integument, including direct preservation [3,6,7], quill knobs on the ulna [8], and even specialized vertebrae that form a pygostyle tail structure [9–13]. Yet more specimens have shown that these dinosaurs actively brooded over their nests [14–19] with an intermediate strategy between those used by crocodilians and extant birds [20], and even had avian-like brain organization [21,22], though see [23] for a more detailed examination of this topic. Based on known cranial morphology, this diverse clade contained both omnivorous and herbivorous members [13,24–26].

Almost all of the aforementioned discoveries were made in Asia, and thus understanding of true diversity across their entire range was incomplete . Over the past few decades, paleontologists have discovered multiple new North American species, leading to a better understanding of morphology and interrelationships [13,27–34]. Specifically, all North American

oviraptorosaurs fall within Caenagnathidae [13,27,30,34–37], which also includes members from Asia [5,31], during the Late Cretaceous. A slender manus, gracile, long hindlimbs, and distinctive mandibles with edentulous beaks in place of the toothed jaws seen in other theropods all characterize this group[27,32]. North American caenagnathid fossils are often found as isolated elements or are poorly preserved, and thus historically paleontologists misidentified them as members of other clades [38]. However, a number of discoveries over the past few decades have led to an improved understanding of Caenagnathidae and its relationships to other members of Oviraptorosauria [13,27–29,37,39].

Still, understanding remains plagued by the relative incompleteness of most specimens, with most named taxa known only from very sparse material [27,29,33,35–37]. This makes studying issues such as ontogeny and other aspects of growth related variation within species quite difficult [38], though paleontologists have found eggshell possibly referable to this family [40]. Previous studies have focused on osteohistology of individual, often isolated elements such as single limb bones [5,41], or isolated mandibles [42], though Cullen et al. (2020) [38] examined multiple elements of the same specimen. Cullen et al. 2020 [38] utilized a series of characters linking the still-fragmentary specimen ROM VP 65884 to the family Caenagnathidae, and referred the specimen to the taxon *Anzu wyliei* based on size and provenance, despite sharing no autapomorphies with *A. wyliei*. Cullen et al. 2020 emphasized the importance of using osteohistological methods where possible when trying to assign fragmentary specimens to existing species or genera, because taxa differ massively in size [5,37], and it is possible to bias estimates of diversity if size alone is used as an indicator of taxonomic affinity.

In the study presented here, I build upon the methodology used by Cullen et al. [38], and apply it to a new specimen that I refer to Caenagnathidae based on provenance and caenagnathid

morphological characters. I utilized information from Cullen et al. [38], and personal communications with the original authors (M. Lamanna, pers. comm.). Here, I describe this specimen, and I look for multiple osteohistological correlates for age and relative maturity at the time of death, to determine whether or not this specimen may reliably be considered the first true juvenile specimen of *Anzu wyliei*, or a specimen of another, smaller caenagnathid species yet to be described from the Hell Creek Formation.

MATERIALS AND METHODS

All bones were prepared prior to acquisition. Bones were photographed from lateral, medial, anterior, posterior, proximal, and distal ends. Each view was removed from its background and placed into a plate to scale for better comparison. In order to eliminate issues of poor lighting in the photographing environment, the brightness of the objects was increased by 100 in Adobe Photoshop 2021 for each image to avoid introduction of bias. Measurements of bones were taken using a flexible tape measure to the nearest millimeter (Table 1). Measurements were taken from proximalmost to distalmost point of the element. Other measurements such as proximal and distal width were taken digitally using prepared figures (specifically Figure 1A and 1B in case of the femur) and ImageJ. Because of taphonomic distortion of the cnemial crest, a proximal width measurement is unreliable and thus was not taken.

Paleontological ethics statements

This section follows the format of Lamanna et al. 2014 [13]. The specimen described in this paper (CM 96523) is permanently reposited in the collections of the Section of Vertebrate Paleontology at Carnegie Museum of Natural History (CM), 4400 Forbes Avenue, Pittsburgh,

Pennsylvania, United States of America. The locality information for this specimen is on file in the Section of Vertebrate Paleontology at Carnegie Museum of Natural History. No permits were required for the described study, which complied with all relevant regulations. All specimens were collected from privately-owned land in the United States of America with the written consent of the respective landowners, and were purchased by the primary author for donation to the Carnegie Museum.

Institutional Abbreviations

BHM, Black Hills Institute of Geological Research, Hill City, South Dakota, United States of America; CM, Carnegie Museum of Natural History, Pittsburgh, Pennsylvania, United States of America; FMNH, Field Museum of Natural History, Chicago, Illinois, United States of America; IGM, Institute of Geology, Ulaanbaatar, Mongolia; MRF, Marmarth Research Foundation, Marmarth, North Dakota, United States of America; OMNH, Sam Noble Oklahoma Museum of Natural History, Norman, Oklahoma, United States of America; ROM, Royal Ontario Museum, Toronto, Ontario, Canada.

Histological Sectioning

The region containing the minimum circumference within the mid-diaphysis of the femur, tibia, and metatarsal IV was selected for removal and thin section processing, following the procedures outlined in Lamm (2013) [43]. Lines of minimum circumference were marked with a red china pencil. Prior to sample removal each bone was: photographed in anterior, posterior, lateral, and medial orientations; bone shape was outlined on paper; and each bone was 3D laser scanned using a NextEngine Ultra HD scanner. Finally, plaster cradles were made for each specimen.

Transverse samples that included the minimum diaphysis circumference were removed using a wet tile saw fitted with a continuous rim diamond blade. On either side of the sample removed, the specimen suffered a small amount of kerf loss from the blade. Thus, a small break was forced upon nearly completing each transverse cut through the shafts, to ensure one area on each side of the sample matched up to the rest of the diaphysis, to preserve the original length of the bone once the cast was produced. Each sample removed was then molded using Douglas and Sturgess 2-part Silputty, and cast using Smooth-On Smooth-Cast 321 two part resin. Casts were primed and painted to resemble the appearance of the removed samples. The cast replicas were not restored to the bone shafts, but placed in the specimen cradles where the original pieces were removed. The portion of the cast representing the forced break in the samples contacted with the remainder of the specimen, ensuring no loss in length in each case with inclusion of the replica.

The sample removed was indicated on each drawn specimen outline, and the samples were then embedded in Silmar two-part polyester resin (Sil95BA-41). After the resin cured, the samples were processed using a Buehler Isomet 1000 precision saw, with a diamond wafering blade, to obtain two, 2mm thick transverse wafers to either side of the minimum diaphysis. For each sample, one surface of each wafer was then polished on a Buehler Ecomet 4 variable speed polisher/grinder with 600 grit and then 800 grit silicon carbide paper to remove marks left by the wafering blade. The polished side of the wafers were then glued to frosted plastic slides using cyanoacrylate glue (Starbond, medium viscosity) and left to cure for 48 hours. Each slide was then polished on the Ecomet 4 using silicon carbide papers of progressively finer grit (60 to 1200), and given a final hand polish using a 1 micron cloth and first a 5 micron slurry and then a 1 micron aluminum oxide gel. In this way, two thin section slides were produced from the midshaft diaphysis of each specimen.

Each completed thin section was analyzed using a Nikon Eclipse polarizing microscope under plane, circular, and full wave-plate polarization. Whole thin section photomontages were produced using an ASI motorized stage and Nikon DS-Ri2 camera affixed to the microscope at 50X total magnification, and with the software package Nikon Elements: Documentation. The resulting digital image of the femur and tibia were used to restore the original shapes of the diaphyseal sections. Digital restoration was performed in Adobe Photoshop CC. Digital LAG and surface tracing was also performed in Photoshop for all three bones (which included the digitally reconstructed femur and tibia). Each LAG, where visible, was digitally traced on a Photoshop layer using a blue line, and a red line was used to indicate a region where LAG tracings and surface tracings had to be estimated because of cortical drift, crushing, or missing cortex. Diaphyseal circumferences were quantified using Fiji [44].

Mass Estimation

In order to get a mass estimate for CM 96523, I needed to obtain a femoral circumference estimate, accounting for taphonomic distortion. This was done using images of femoral cross sections of other Oviraptorosaur taxa such as *Oksoko* and *Apatoraptor* provided by Dr. Gregory Funston. Dr. Holly Woodward was able to use this information to restore the cross section of the femur using the slice that she cut for histological analysis. I then plotted this estimate against regressions of body mass versus stylopodial circumference made by Campione and others [45] to obtain a range of plausible body masses for this specimen. I did the same for *Anzu*, using the femoral circumference of CM 78000 provided by Lamanna et al. [13] so I could compare body masses using the same method of estimation.

RESULTS

Systematic Paleontology

Theropoda Marsh 1881 [46]

Oviraptorosauria Barsbold 1976 [47]

Caenagnathidae Sternberg 1940 [48]

Caenagnathidae indet.

Material. CM 96523, a set of partial hindlimbs consisting of a left femur, right tibia and astragalocalcaneum, a right metatarsal III, and a right metatarsal IV.

Locality and Horizon: South Dakota, United States of America. Upper Cretaceous (upper Maastrichtian [49]) Hell Creek Formation. Though the specimen was prepared prior to acquisition, some regions such as the proximal portion of the tibia and anterodistal region of the femur still preserve original matrix, which resembles that of typical floodplain deposits seen in the Hell Creek Formation (pers. obs.), as suggested of the type specimens of *Anzu wyliei* [13].

Taxonomic Comments: In order to provide a a taxonomic identification for the specimen, I followed the methods used by Cullen et al. (2020) on specimen ROM VP 65884, and scored CM 96523 for the data matrix of Funston and Currie (2020). I then compared character state scores to other oviraptorosaurs, particularly focusing on *Anzu wyliei*. Several characters on the metatarsus of ROM VP 65884, noted to be diagnostic of the clade Caenagnathidae [38], are shared with CM 96523. Specifically, the anteroposteriorly flattened metatarsal III, the prominent and deep concavity on the posterior surface of the tarsometatarsus, and the cruciate ridges on both sides of metatarsal III are diagnostic of the clade Caenagnathidae. While the incompleteness the specimen makes it impossible to place within the family with any great precision, the data

provided supports the hypothesis that the specimen is nested within Caenagnathidae and does not represent some other theropod (See Supplementary Info).

Description and Comparisons

The new specimen, CM 96523, consists of a left femur, a right tibia and astragalocalcaneum, one right metatarsal III, and one right metatarsal IV. Both the femur and tibia are highly crushed along their shafts, both are nearly flattened when viewed from lateral or medial perspectives. However, proximal and distal ends of these two bones remain relatively unaltered, though fragmentation of the bone surface is present, likely caused by pressure undergone during the fossilization process. In contrast, the two preserved metatarsals show no signs of crushing, and are entirely unbroken aside from a few small cracks. All bones are highly laminate and smooth, though there is a clear change in surface texture on articular surfaces and areas of muscle or ligament attachment.

Table 1. Measurements (in mm) of preserved elements of CM 96523.

Bone	**Femur**	**Tibia +Astragalocalcaneum**	**Mt III**	**Mt IV**
Length	342	480	247	233
Circumference [est]	105.8	106.8	-	64.2
Proximal width	109	-	15	21
Distal width	85	70	21	15

Femur

The femur of CM 96523 is shorter than any complete femora assigned to *Anzu wyliei* [13], but is similar in length to known specimens of cf. *Caenagnathus collinsi* and *Chirostenotes*

pergracilis [33]. The distal and proximal ends are still well-preserved enough to determine several anatomical features (Fig 1). The femoral head has a series of distinct and highly prominent furrows, indicating a rather prominent cartilaginous epiphysis - these furrows are not quite as prominent in CM 78000 or CM 78001. Furthermore, the long axis of the head and neck meets the shaft at a marginally obtuse angle of approximately 100°, compared to the 90° angle described in *Anzu wyliei* [13]. The distal condyles of CM 96523 are not nearly as expansive as observed in the *Anzu* type specimens – this may be an artefact of the smaller size of the element.

As in the *Anzu* type specimens, there is little to no separation between the greater trochanter and femoral head, and it appears that the anterior and greater trochanters form an accessory trochanteric crest, though it is difficult to say for certain. It is possible to say with relative confidence that there is either no fourth trochanter, or if present it is extremely weakly developed, as there are no shaft fragments that, when assembled together, would create the distinctive crest-like shape of such a feature. The adductor fossa and the associated anteromedial crest on the distal femur do appear to be well-developed, as seen in the *Anzu* type specimens, though not quite to the same degree; the fibular condyle also projects slightly beyond the tibial condyle.

Tibia and Astragalocalcaneum

The tibia is a long and slender element - the ratio of the distal condyle width to the proximodistal length is less than 0.20, and the tibia is 1.40 times longer than the femur, differing from the proportions seen in CM 78000 and CM 78001, where the tibia is between 1.25 and 1.17 times longer than the femur respectively [13]. This high ratio compares well with *Elmisaurus rarus* specimen IGM 102/7, with a ratio of 1.39 [50].

The astragalus and calcaneum appear to be fused into a single element as is seen in *Anzu wyliei* [13] (Fig 2), but this element itself may be fused to the end of the tibia, a trait that is quite rare in oviraptorosaurs (Greg Funston, pers. comm., 2020). It appears that the ascending process of the astragalus would have been taller than wide. it is difficult to determine with certainty whether or not there is a tubercle on the astragalocalcaneum as there is in *Anzu* [13], because of surface fragmentation.

Metatarsals

The two metatarsals found in CM 96523 cannot be compared to the type series of *Anzu wyliei*, as no weight-bearing metatarsals were preserved in these specimens. While a partial set of weight-bearing metatarsals were associated with ROM VP 65884, referred by Cullen et al. to cf. *Anzu wyliei* [38], none of the three were complete; all were missing the proximal ends and distal condyles. In contrast, the two metatarsals preserved with CM 96523 are complete, with both proximal and distal ends intact. The metatarsals are elongate, being over 3 times longer than their proximal width, even accounting for the width of the missing metatarsal II. They are also quite long in proportion to the proximal elements of the hindlimb, measuring 0.7-0.8 times the length of the femur, though slightly more than half the length of the tibia. The two metatarsals included with this specimen correspond to metatarsals III and IV, from the right hindlimb. Neither bones show any sign of coossification into a single element as seen in some other caenagnathids such as *Citipes elegans* [33,35,51].

Metatarsal III

Metatarsal III is highly constricted proximally, reaching its mediolaterally narrowest point approximately a quarter of the way down from the proximal articular surface, before slowly widening before again slightly constricting immediately proximal to the distal articular

surface (Fig 3). This is indicative of an arctometatarsalian condition, though based on the morphology it seems likely that only the proximalmost portion of metatarsal III would be obscured as seen in *Citipes elegans* [31,33]. The bone compares quite favorably to the morphology seen in the less complete metatarsals of ROM VP 65884 [38]. The metatarsal is anteroposteriorly flattened, with a concave posterior surface. Furthermore, this posterior surface has sharp medial and lateral longitudinal ridges, continuous with lateral and medial postcondylar ridges respectively; together, these form a chiasmata, as seen in *Citipes elegans* specimens, but not in *Chirostenotes pergracilis* [31].

Metatarsal IV

Metatarsal IV appears typical for such an element among caenagnathids, with a slightly deflected distal end as observed in left Mt IV of ROM VP 65884 [38]. Distal tarsal IV is fused to the proximolateral end of the bone, as is seen in species such as *Elmisaurus rarus* [35,50] and *Citipes elegans* [33]; however, the proximodorsal process of this element is broken (Fig 4). The proximal articular surface has a semitriangular facet on its medial side, presumably for articulation with Mt III. A highly pronounced ridge runs from the lateral edge of the proximal articular surface, continuing distally to form the ridge ventral to the lateral ligament pit. However, this ridge does not form a pointed process on the proximal articular surface. This ridge appears rugose and is likely the insertion scar for the *M. gastrocnemius pars lateralis* [52]. The articular surface for Mt III is elongate along the medial margin of Mt IV, extending proximally from the proximoventral edge of the medial ligament pit, with anteroposterior enlargement of the contact at its distal end and slowly tapering proximally. This articular surface extends over 70% of the shaft of metatarsal IV. There is also a somewhat rugose surface on the proximal anterior

edge of the metatarsal - comparison to other theropods leads us to believe this is an insertion for the *M. tibialis anterior* [52,53].

Histology

Femur:

The diaphysis was crushed in the anterior-posterior direction post-burial, but cortical microstructural preservation is such that histological descriptions can still be made. There is a well-developed and complete lamellar endosteal layer, with frequent simple radial vascular canals traveling between the medullary cavity and inner cortex (Fig 5). The primary cortex is fibrolamellar and vascular canals are reticular and sub-laminar. Osteocyte lacunae density is high throughout the cortex. Anterolaterally from inner to outer cortex there is a localized column of secondary osteons, likely related to a tendon enthesis. No secondary osteons are present outside of this column of remodeled bone. Six LAGs are visible. The innermost LAG is only partially present, having been resorbed by medullary expansion. There is no remarkable evidence of cortical drift. The zone of primary tissue between the innermost LAG and the next comprises the majority of the cortex. Thereafter, the zones between LAGs 2-6 are more closely-spaced (Table 2, Fig 5). After the fifth LAG, vascular density is greatly decreased, although osteocyte lacunae density remains high. After the fifth LAG, bone tissue is also loosely parallel-fibered. From the retrodeformed transverse thin section image, femoral shaft circumference is 105.8 mm.

Table 2. Comparison of relative growth for histologically sampled elements of CM 96523. MC: medullary cavity.

Element	Growth Zone	Relative % of cortex

Femur (undeformed)	Medullary cavity to LAG 1	Lost to MC expansion
	LAG 1 to LAG 2	6.17
	LAG 2 to LAG 3	14.20
	LAG 3 to LAG 4	3.09
	LAG 4 to LAG 5	2.47
	LAG 5 to LAG 6	1.23
	LAG 6 to outer surface	1.23
Tibia	Medullary cavity to LAG 1	6.40
	LAG 1 to LAG 2	11.63
	LAG 2 to LAG 3	2.33
	LAG 3 to LAG 4	2.91
	LAG 4 to LAG 5	1.74
	LAG 5 to LAG 6 (not traceable)	0.58
	LAG 6 to outer surface	0.58
Metatarsal IV	Medullary cavity to LAG 1	4.91
	LAG 1 to LAG 2	31.89
	LAG 2 to LAG 3	13.54
*	LAG 3 to LAG 4	2.06
*	LAG 4 to LAG 5	2.55
*	LAG 5 to LAG 6	2.16
	LAG 6 to outer surface	1.57

*Some estimation required to trace LAG.

Tibia:

As with the femur, the tibia diaphysis was crushed in the anterior-posterior direction post-burial, but a histological description is still possible. The lamellar endosteal layer is well-developed, with frequent simple radial vascular canals traveling between the medullary cavity and inner cortex (Fig 6). The primary cortex is fibrolamellar and vascular canals within inner and mid-cortex are a combination of reticular and longitudinal, with frequent short radial anastomoses. Longitudinal vascularity dominates within the outer cortex. No secondary osteons are observed. The first visible LAG is located within the mid-cortex, and the tissue from the endosteal surface to the second LAG comprises the majority of the cortex (Table 2). The first LAG is only partially visible, having been largely eroded by medullary cavity expansion. Cortical drift, however, is negligible. The zones between LAGs 2-6 towards the periosteal surface are markedly thinner (Fig 6). Vascular density is also reduced in these last four zones, but only slightly. The sixth LAG is so close to the periosteal surface that it often merges with it. From the retrodeformed thin section image, transverse section tibia circumference is 106.8 mm.

Metatarsal IV:

There is a well-developed lamellar endosteal layer, and occasional simple radial vascular canals pass between the medullary cavity and primary cortex (Fig 7). Primary tissue from inner to outer cortex is fibrolamellar with a high density of osteocyte lacunae. Vascular canal density is somewhat higher in the innermost cortex compared with the mid- and outer cortex. Anteromedially, canals are primarily a combination of longitudinal and reticular, and are largely sub-laminar elsewhere. Posteriorly within the innermost cortex there is a crescent of compact coarse cancellous bone (CCCB) [54] between the lamellar endosteal layer and the periosteally-derived mid-cortex. On the medial and lateral sides, a localized column of secondary osteons

spans from inner to outer cortex, likely related to ligamentous entheses. Beyond these columns, no secondary osteons are present within the cortex. A nutrient foramen is present near the periosteal surface on the medial side.

Within the outer cortex, vascular density is decreased, consisting of scattered longitudinal and reticular vascular canals. Osteocyte lacunae density remains high in the outermost cortex on the anterior side, and is less dense with more flattened lacunae on the posterior side. Six LAGs are present. Three widely-spaced LAGs are visible within the cortex, with the innermost only partially visible, as medullary cavity expansion caused its erosion. LAG spacing is then abruptly decreased between the final three LAGs nearest the periosteal surface. LAGs 4-6 are traceable, but merge with the periosteal surface in places (Table 2, Fig. 6). Although the primary tissue within these outer three zones is fibrolamellar on the anterior side, the tissue is parallel-fibered to lamellar on the posterior side. An overlay of LAG tracings reveals very little cortical drift over ontogeny. Transverse thin section circumference is 64.2 mm.

Mass Estimation

With an estimated femoral circumference of 105.8mm, the body mass interval predicted for CM 96523 is 58.9 - 98.1 kg. This is far less than predicted for CM 78000, with an estimated body mass between 202 and 342 kg. It likely would have been comparable in size to the ‘mid-sized’ caenagnathids from the earlier Dinosaur Park Formation (Greg Funston, pers. comm. 2020).

DISCUSSION

Histology

CM 96523 represents only the fourth instance of published caenagnathid long bone histoanalyses [38,41,42], and is the first assessment of caenagnathid femoral histology. The femur, tibia, and metatarsal IV of CM 96523 each record six LAGs, although the large medullary cavities of the bone may have obliterated one or more LAGs as they expanded. At minimum, the individual was six years of age when it died. Because the sixth LAG is so close to the periosteal surface and often merges with the surface in each bone examined, it is likely this individual died shortly after emerging from its annual growth hiatus.

LAG spacing reveals that the majority of bone apposition and body size increase occurred during the first 2 recorded years of age, based on femur and tibia histology. After the second LAG, there is a marked shift to closely spaced LAGs, comprising the remainder of the outer cortex. This inflection in apposition rate may correspond to sexual maturity, as has been hypothesized for other dinosaur groups including oviraptorosaurs [55–57]. Interestingly, apposition rate inflection occurred after the third recorded year within metatarsal IV, rather than in the second recorded year as observed in the femur and tibia. This may reflect differing apposition rates for different parts of the hindlimb.

The tibia histology of CM 96523 differs from that of a previously described indeterminate caenagnathid (UALVP 57349) from the Campanian-early Maastrichtian Horseshoe Canyon Formation in Alberta, Canada. The histology of UALVP 57349 suggests this small individual (tibia length of 210 mm) was a young juvenile. Its bone tissue is entirely reticular and plexiform fibrolamellar, with open vascular canals at the periosteal surface, no

secondary osteons, and an avascular endosteal lamellar layer. A band of parallel-fibered tissue within the cortex may be an annulus, suggesting it was at least one year of age [41]. The larger tibia of CM 96523 (480mm) described here is also entirely fibrolamellar, but vascular orientation is reticular to sub-laminar, has a vascularized lamellar endosteal layer, and there are six well-defined LAGs within the cortex. Beginning with the fourth LAG, zonal spacing between LAGs is markedly decreased towards the periosteal surface, and the vascular canals are not open at the bone surface. The histology of UALVP 57349 and CM 96523 show that the tibia of each was still growing when the individuals died. However, the histology of CM 96523 suggests it was relatively older (six LAGs compared to a single annulus) and growth was approaching an asymptote, whereas UALVP 57349 shows no indication of decreasing annual apposition rate.

The histology of CM 96523 also differs from the larger tibia of ROM VP 65884, referred to *Anzu wyliei* [38] from the Maastrichtian Hell Creek Formation of Montana. Although the main tissues in both tibiae are fibrolamellar, the vascularity in ROM VP 65884 spans from reticular within the inner cortex to plexiform in the outer cortex, while that of CM 96523 is a combination of reticular and longitudinal for most of the cortex to predominantly longitudinal in the outermost cortex. ROM VP 65884 preserves seven LAGs, with a noticeable decrease in zonal spacing occurring after the third LAG. The tibia of CM 96523 preserves only six LAGs, with a pronounced decrease in zonal thickness occurring after the second LAG. Finally, although zonal spacing is decreased within the outer zones of the larger tibia of ROM VP 65884, tissue remains well-vascularized to the periosteal surface and there is no indication an EFS is present. This differs from CM 96523, which exhibits reduced, longitudinal vascularity within the outermost cortical zones.

Vascular orientation can be compared to determine relative growth rates [58]. Longitudinal vascular canals within the outermost zones of tibia CM 96523 indicate a slower annual growth rate than the plexiform vascularity observed in tibia ROM VP 65884, referred to *A. wyliei.* Although I cannot discount individual growth variation (e.g., Woodward et al. 2015 [59]), it appears that CM 96523 would have attained a smaller asymptotic body size than reported for specimens of *A. wyliei* [13,38].

The metatarsal IV histology of CM 96523 resembles that of the Campanian-aged Dinosaur Park Formation *Citipes elegans* metatarsal IV (UALVP 59606) described previously by Funston et al. (2020) [42]. In both, the bone tissue is reticular to longitudinal fibrolamellar, the lamellar endosteal layer is pierced by vascular canals, and the cortex preserves six LAGs. The two metatarsals differ in that the LAG spacing in *C. elegans* metatarsal IV becomes reduced after the second LAG, while this occurs after the third LAG in CM 96523. Also, the metatarsal IV of *C. elegans* (total length of 146 mm) contained secondary osteons, and the closely spaced LAGs within avascular outermost cortex was interpreted as an EFS and signaling skeletal maturity [42]. In contrast, the zones between the closely spaced outermost LAGs in metatarsal IV of CM 96523 (total length of 233mm) remain vascularized with high osteocyte density, suggesting that this larger metatarsal was approaching asymptotic length but was still growing in length at death.

Overall Findings

The results from histological sectioning suggest that this animal was of subadult or adult status at the time of its death, contrary to what we would expect if this specimen were a juvenile *Anzu wyliei*. In addition to histological data, CM 96523 differs from *Anzu wyliei* in having distal tarsals fused to the metatarsus, a lack of exclusion of the astragalus from the lateral margin of the

tarsus, and a pointed process on the proximolateral edge of Mt IV. For these reasons, I suggest that the specimen should not be referred to *Anzu wyliei* and instead posit that CM 96523 represents a new, smaller caenagnathid from the Hell Creek Formation. These results further highlight the importance of taking histological data into account when assigning taxonomic identities to incomplete caenagnathid remains, reinforcing the point originally made by Cullen et al. 2020 [38]. Hopefully, more diagnostic remains of this smaller Hell Creek caenagnathid species will be described in time, but until then I refer to it as Caenagnathidae indet., or, informally, the "KLAW caenagnathid."

Given this, it appears that multiple species of caenagnathid coexisted during the end-Maastrichtian, which is not entirely unexpected given the Campanian Dinosaur Park Formation preserves as many as three caenagnathid taxa within the same ecosystem, each of a different adult size [33]. In the Dinosaur Park Formation, the largest species, *Caenagnathus collinsi*, approached *Anzu wyliei* in size [33,34]. However, there were also two smaller taxa, *Chirostenotes pergracilis* and *Citipes elegans*. The KLAW caenagnathid appears to conform to *Chirostenotes* in size. However, *Citipes* lacks proximal hindlimb material such as tibiae or femora so it is hard to compare, though it seems to have been the smallest caenagnathid within the Dinosaur Park Formation [33]. Unfortunately, little is known about the ecology of each species, though it has been posited based on mandibular morphology that *Chirostenotes* was an omnivore based on mandibular morphology [32]. However, the morphology of *Anzu* is different from that of *Chirostenotes* [13], and as such I cannot make the same inferences with certainty, though omnivory certainly seems plausible given its size; even without a particularly strong grasping jaw, it would be able to swallow whole many of the smaller vertebrates found in its environment. I cannot assess this matter in the KLAW caenagnathid as it lacks a skull, but given

the versatility of an omnivorous diet it seems a reasonable possibility, though not fair to assume completely.

CONCLUSIONS

In conclusion, I have confirmed via histology and several osteological characters that the new specimen CM 96523 does not represent a juvenile specimen of *Anzu wyliei*, but rather a new, undescribed caenaganthid taxon from the Hell Creek Formation. I further emphasize the importance of using histological examination rather than size alone to infer taxonomy, as was previously written in Cullen et al. [38]. I briefly touch upon the issues of coexistence of two caenagnathids existing in the Hell Creek, though note that earlier formations had as many as 3 coexisting taxa. The ecology of this group is a subject that is still poorly understood and requires further research to elucidate.

REFERENCES

1. Osmólska H. Oviraptorosauria. In: Weishampel D, Dodson P, Osmólska H, editors. The dinosauria. Berkeley, CA: University of California Press; 2004. pp. 165–183.
2. Funston GF, Chinzorig T, Tsogtbaatar K, Kobayashi Y, Sullivan C, Currie PJ. A new two-fingered dinosaur sheds light on the radiation of Oviraptorosauria. R Soc Open Sci. 7: 201184. doi:10.1098/rsos.201184
3. Qiang J, Currie PJ, Norell MA, Shu-An J. Two feathered dinosaurs from northeastern China. Nature. 1998;393: 753–761. doi:10.1038/31635
4. Lü J, Currie PJ, Xu L, Zhang X, Pu H, Jia S. Chicken-sized oviraptorid dinosaurs from central China and their ontogenetic implications. Naturwissenschaften. 2013;100: 165–175. doi:10.1007/s00114-012-1007-0
5. Xu X, Tan Q, Wang J, Zhao X, Tan L. A gigantic bird-like dinosaur from the Late Cretaceous of China. Nature. 2007;447: 844–847. doi:10.1038/nature05849
6. Zhou Z-H, Wang X-L, Zhang F-C, Xu X. Important features of *Caudipteryx* - evidence from two nearly complete new specimens. Vertebr Palasiat. 2000;38: 242–254.
7. Xu X, Zheng X, You H. Exceptional dinosaur fossils show ontogenetic development of early feathers. Nature. 2010;464: 1338–1341. doi:10.1038/nature08965
8. Kurzanov S. Structural characteristics of the fore limbs of *Avimimus*. Paleontol J. 1982;1982: 108–112.

9. Barsbold R, Currie PJ, Myhrvold NP, Osmólska H, Tsogtbaatar K, Watabe M. A pygostyle from a non-avian theropod. Nature. 2000;403: 155–156. doi:10.1038/35003103
10. Barsbold R, Osmólska H, Watabe M, Currie PJ, Tsogtbaatar K. A new oviraptorosaur (Dinosauria, Theropoda) from Mongolia: the first dinosaur with a pygostyle. Acta Palaeontol Pol. 2000;45: 97–106.
11. He T, Wang X-L, Zhou Z-H. A new genus and species of caudipterid dinosaur from the lower cretaceous Jiufotang Formation of western Liaoning, China. Vertebr Palasiat. 2008;46: 178–189.
12. Persons IV S, Currie PJ, Norell MA. Oviraptorosaur tail forms and functions. Acta Palaeontol Pol. 2013;59: 553–567. doi:10.4202/app.2012.0093
13. Lamanna MC, Sues H-D, Schachner ER, Lyson TR. A new large-bodied oviraptorosaurian theropod dinosaur from the latest Cretaceous of western North America. PLoS One. 2014;9: e92022.
14. Osborn H. Three new Theropoda, Protoceratops zone, central Mongolia. Am Mus Novit. 1924;144: 1–12.
15. Norell MA, Clark JM, Chiappe LM, Dashzeveg D. A nesting dinosaur. Nature. 378: 774–776.
16. Dong Z-M, Currie PJ. On the discovery of an oviraptorid skeleton on a nest of eggs at Bayan Mandahu, Inner Mongolia, People's Republic of China. Can J Earth Sci. 1996;33: 631–636. doi:10.1139/e96-046
17. Clark JM, Norell M, Chiappe LM, Project M-AMP, Akademi MSU. An oviraptorid skeleton from the late Cretaceous of Ukhaa Tolgod, Mongolia, preserved in an avianlike brooding position over an oviraptorid nest. American Museum novitates ; no. 3265. 1999 [cited 18 Nov 2020]. Available: http://digitallibrary.amnh.org/handle/2246/3102
18. Varricchio DJ, Moore JR, Erickson GM, Norell MA, Jackson FD, Borkowski JJ. Avian paternal care had dinosaur origin. Science. 2008;322: 1826–1828. doi:10.1126/science.1163245
19. Fanti F, Currie PJ, Badamgarav D. New Specimens of *Nemegtomaia* from the Baruungoyot and Nemegt Formations (Late Cretaceous) of Mongolia. PLOS ONE. 2012;7: e31330. doi:10.1371/journal.pone.0031330
20. Sato T, Cheng Y-N, Wu X, Zelenitsky DK, Hsiao Y. A pair of shelled eggs inside a female dinosaur. Science. 2005;308: 375–375. doi:10.1126/science.1110578
21. Osmólska H. Evidence on relation of brain to endocranial cavity in oviraptorid dinosaurs. Acta Palaeontol Pol. 2004;49: 321–324.
22. Kundrát M. Avian-like attributes of a virtual brain model of the oviraptorid theropod *Conchoraptor gracilis*. Naturwissenschaften. 2007;94: 499–504. doi:10.1007/s00114-007-0219-1
23. Balanoff AM, Bever GS, Rowe TB, Norell MA. Evolutionary origins of the avian brain. Nature. 2013;501: 93–96. doi:10.1038/nature12424
24. Xu X, Cheng Y-N, Wang X-L, Chang C-H. An unusual oviraptorosaurian dinosaur from China. Nature. 2002;419: 291–293. doi:10.1038/nature00966
25. Smith D. The type specimen of *Oviraptor philoceratops*, a theropod dinosaur from the Upper Cretaceous of Mongolia. Neues Jahrb Für Geol Paläontologie Abh. 1992;186: 365–388.
26. Zhou Z-H, Wang X-L. A new species of *Caudipteryx* from the Yixian Formation of Liaoning, Northeast China. Vertebr Palasiat. 38.

27. Currie PJ, Russell DA. Osteology and relationships of *Chirostenotes pergracilis* (Saurischia, Theropoda) from the Judith River (Oldman) Formation of Alberta, Canada. Can J Earth Sci. 1988;25: 972–986. doi:10.1139/e88-097
28. Sues H-D. On *Chirostenotes*, a Late Cretaceous Oviraptorosaur (Dinosauria: Theropoda) from Western North America. J Vertebr Paleontol. 1997;17: 698–716.
29. Zanno LE, Sampson SD. A new oviraptorosaur (Theropoda, Maniraptora) from the Late Cretaceous (Campanian) of Utah. J Vertebr Paleontol. 2005;25: 897–904.
30. Currie PJ, Godfrey SJ, Nessov L. New caenagnathid (Dinosauria: Theropoda) specimens from the Upper Cretaceous of North America and Asia. Can J Earth Sci. 1993;30: 2255–2272. doi:10.1139/e93-196
31. Funston GF, Currie PJ, Burns ME. New elmisaurine specimens from North America and their relationship to the Mongolian *Elmisaurus rarus*. Acta Palaeontol Pol. 2015;61: 159–173. doi:10.4202/app.00129.2014
32. Funston GF, Currie PJ. A previously undescribed caenagnathid mandible from the late Campanian of Alberta, and insights into the diet of *Chirostenotes pergracilis* (Dinosauria: Oviraptorosauria). Sues H, editor. Can J Earth Sci. 2014;51: 156–165. doi:10.1139/cjes-2013-0186
33. Funston G. Caenagnathids of the Dinosaur Park Formation (Campanian) of Alberta, Canada: anatomy, osteohistology, taxonomy, and evolution. Vertebr Anat Morphol Palaeontol. 2020;8: 105–153. doi:10.18435/vamp29362
34. Funston GF, Persons IV S, Bradley GJ, Currie PJ. New material of the large-bodied caenagnathid *Caenagnathus collinsi* from the Dinosaur Park Formation of Alberta, Canada. Cretac Res. 2015;54: 179–187. doi:10.1016/j.cretres.2014.12.002
35. Currie PJ. The first records of *Elmisaurus* (Saurischia, Theropoda) from North America. Can J Earth Sci. 1989;26: 1319–1324. doi:10.1139/e89-111
36. Sullivan RM, Jasinski SE. A new caenagnathid *Ojoraptorsaurus boerei*, N. Gen., N. Sp. (Dinosauria, Oviraptorosauria), from the Upper Cretaceous Ojo Alamo Formation (Naashoibito member), San Juan basin, New Mexico. Foss Rec. 2011;3: 418–428.
37. Longrich NR, Barnes K, Clark S, Millar L. Caenagnathidae from the Upper Campanian Aguja Formation of West Texas, and a Revision of the Caenagnathinae. Bull Peabody Mus Nat Hist. 2013;54: 23–49. doi:10.3374/014.054.0102
38. Cullen TM, Simon DJ, Benner EKC, Evans DC. Morphology and osteohistology of a large-bodied caenagnathid (Theropoda, Oviraptorosauria) from the Hell Creek Formation (Montana): implications for size-based classifications and growth reconstruction in theropods. Pap Palaeontol. 2020; 1–17. doi:https://doi.org/10.1002/spp2.1302
39. Funston GF, Currie PJ. A new caenagnathid (Dinosauria: Oviraptorosauria) from the Horseshoe Canyon Formation of Alberta, Canada, and a reevaluation of the relationships of Caenagnathidae. J Vertebr Paleontol. 2016;36: e1160910. doi:10.1080/02724634.2016.1160910
40. Zelenitsky DK, Therrien F, Tanaka K, Currie PJ, DeBuhr CL. Latest Cretaceous eggshell assemblage from the Willow Creek Formation (upper Maastrichtian – lower Paleocene) of Alberta, Canada, reveals higher dinosaur diversity than represented by skeletal remains. Can J Earth Sci. 2017;54: 134–140. doi:10.1139/cjes-2016-0080
41. Funston GF, Currie PJ. A small caenagnathid tibia from the Horseshoe Canyon Formation (Maastrichtian): Implications for growth and lifestyle in oviraptorosaurs. Cretac Res. 2018;92: 220–230. doi:10.1016/j.cretres.2018.08.020

42. Funston GF, Wilkinson RD, Simon DJ, Leblanc AH, Wosik M, Currie PJ. Histology of Caenagnathid (Theropoda, Oviraptorosauria) dentaries and implications for development, ontogenetic edentulism, and taxonomy. Anat Rec. 2020;303: 918–934. doi:10.1002/ar.24205
43. Lamm E-T. Preparation and Sectioning of Specimens. In: Padian K, Lamm E-T, editors. Bone histology of fossil tetrapods: advancing methods, analysis, and interpretation. Berkeley, CA: University of California Press; 2013. pp. 55–160. Available: https://california.universitypressscholarship.com/view/10.1525/california/9780520273528.001.0001/upso-9780520273528-chapter-4
44. Schindelin J, Arganda-Carreras I, Frise E, Kaynig V, Longair M, Pietzsch T, et al. Fiji: an open-source platform for biological-image analysis. Nat Methods. 2012;9: 676–682. doi:10.1038/nmeth.2019
45. Campione NE, Evans DC, Brown CM, Carrano MT. Body mass estimation in non-avian bipeds using a theoretical conversion to quadruped stylopodial proportions. Methods Ecol Evol. 2014;5: 913–923. doi:https://doi.org/10.1111/2041-210X.12226
46. Marsh OC. Principal characters of American Jurassic dinosaurs. Am J Sci. 1878;Series 3 Vol. 16: 411–416. doi:10.2475/ajs.s3-16.95.411
47. Barsbold R. A new Late Cretaceous family of small theropods (Oviraptoridae n. fam.) in Mongolia. Dokl Akad Nauk SSSR. 1976;226: 221–223.
48. Sternberg RM. A toothless bird from the Cretaceous of Alberta. J Paleontol. 1940;14: 81–85.
49. Johnson KR, Nichols DJ, Hartman JH. Hell Creek Formation: a 2001 synthesis. The Hell Creek Formation and the Cretaceous-Tertiary Boundary in the Northern Great Plains: An Integrated Continental Record of the End of the Cretaceous. Geological Society of America; 2002. pp. 503–510.
50. Currie P, Funston G, Osmolska H. New specimens of the crested theropod dinosaur *Elmisaurus rarus* from Mongolia. Acta Palaeontol Pol. 2015 [cited 9 Dec 2020]. doi:10.4202/app.00130.2014
51. Osmólska H. Coossified tarsometatarsi in theropod dinosaurs and their bearing on the problem of bird origins. Palaeontol Pol. 1981;42: 79–95.
52. Carrano MT, Hutchinson JR. Pelvic and hindlimb musculature of *Tyrannosaurus rex* (Dinosauria: Theropoda). J Morphol. 2002;253: 207–228.
53. Hutchinson JR. The evolution of hindlimb tendons and muscles on the line to crown-group birds. Comp Biochem Physiol A Mol Integr Physiol. 2002;133: 1051–1086. doi:10.1016/s1095-6433(02)00158-7
54. Enlow DH. Principles of Bone Remodeling: An Account of Post-Natal Growth and Remodeling Processes in Long Bones and the Mandible. Thomas; 1963.
55. Sander PM. Longbone histology of the Tendaguru sauropods: implications for growth and biology. Paleobiology. 2000;26: 466–488. doi:10.1666/0094-8373(2000)026<0466:LHOTTS>2.0.CO;2
56. Erickson GM, Curry Rogers K, Varricchio DJ, Norell MA, Xu X. Growth patterns in brooding dinosaurs reveals the timing of sexual maturity in non-avian dinosaurs and genesis of the avian condition. Biol Lett. 2007;3: 558–561. doi:10.1098/rsbl.2007.0254
57. Lee AH, Werning S. Sexual maturity in growing dinosaurs does not fit reptilian growth models. Proc Natl Acad Sci. 2008;105: 582–587. doi:10.1073/pnas.0708903105
58. Francillon-Vieillot H, Buffrénil V de, Castanet J, Géraudie J, Meunier FJ, Sire JY,

et al. Microstructure and Mineralization of Vertebrate Skeletal Tissues. Skeletal Biomineralization: Patterns, Processes and Evolutionary Trends. American Geophysical Union (AGU); 1990. pp. 175–234. doi:10.1029/SC005p0175
59. Woodward HN, Fowler EAF, Farlow JO, Horner JR. Maiasaura, a model organism for extinct vertebrate population biology: a large sample statistical assessment of growth dynamics and survivorship. Paleobiology. 2015;41: 503–527. doi:10.1017/pab.2015.19
60. Hendrickx C, Hartman SA, Mateus O. An overview of non-avian theropod discoveries and classification. PalArch's J Vertebr Palaeontol. 2015;12: 1–73.

FIGURES

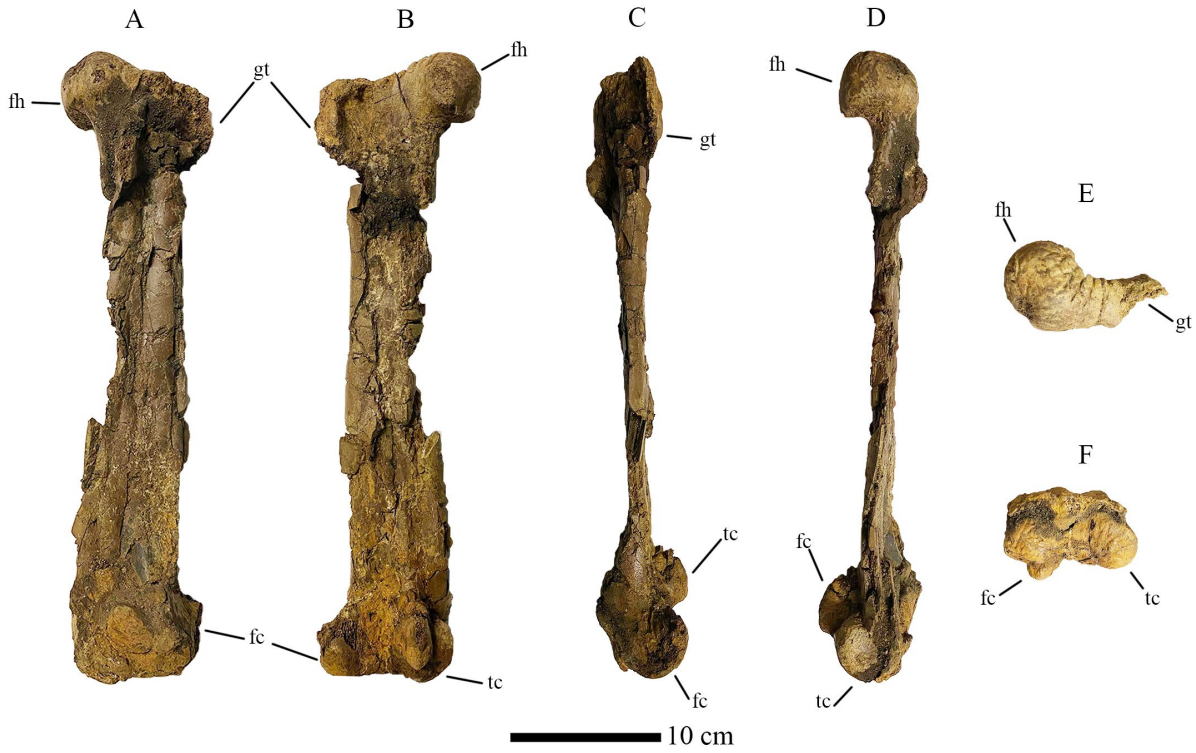

Figure 1. Left femur of CM 96523. Photographs of bone in A) Anterior, B) Posterior, C) Lateral, D) Medial, E) Proximal, and F) Distal views. Note the slightly obtuse angle made by the head and femoral shaft, and prominent furrows in the proximal view. Abbreviations: fc, fibular condyle; fh, femoral head; gt, greater trochanter; tc, tibial condyle. Scale bar = 10cm.

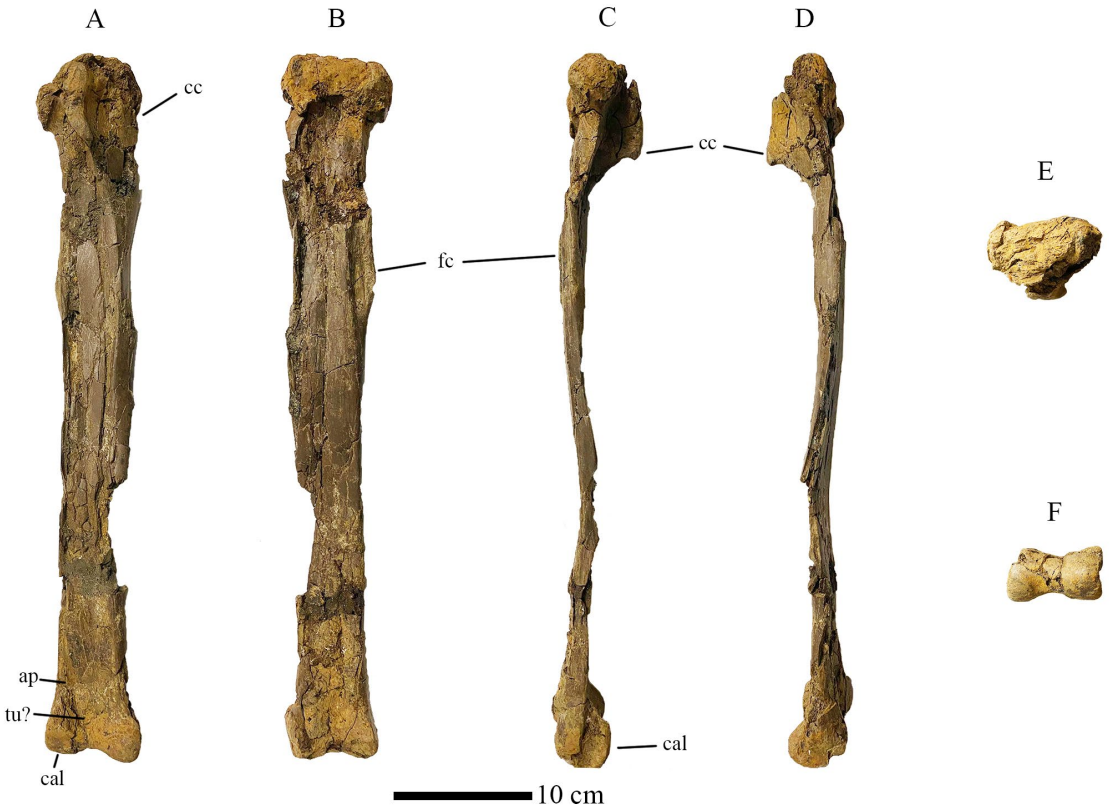

Fig. 2. Right tibia and astragalocalcaneum of CM 96523. Photographs of bone in A) Anterior, B) Posterior, C) Lateral, D) Medial, E) Proximal, and F) Distal views. Abbreviations: ap, ascending process; cal, calcaneum; cc, cnemial crest; fc, fibular crest; tu?, tubercle? Scale bar = 10cm.

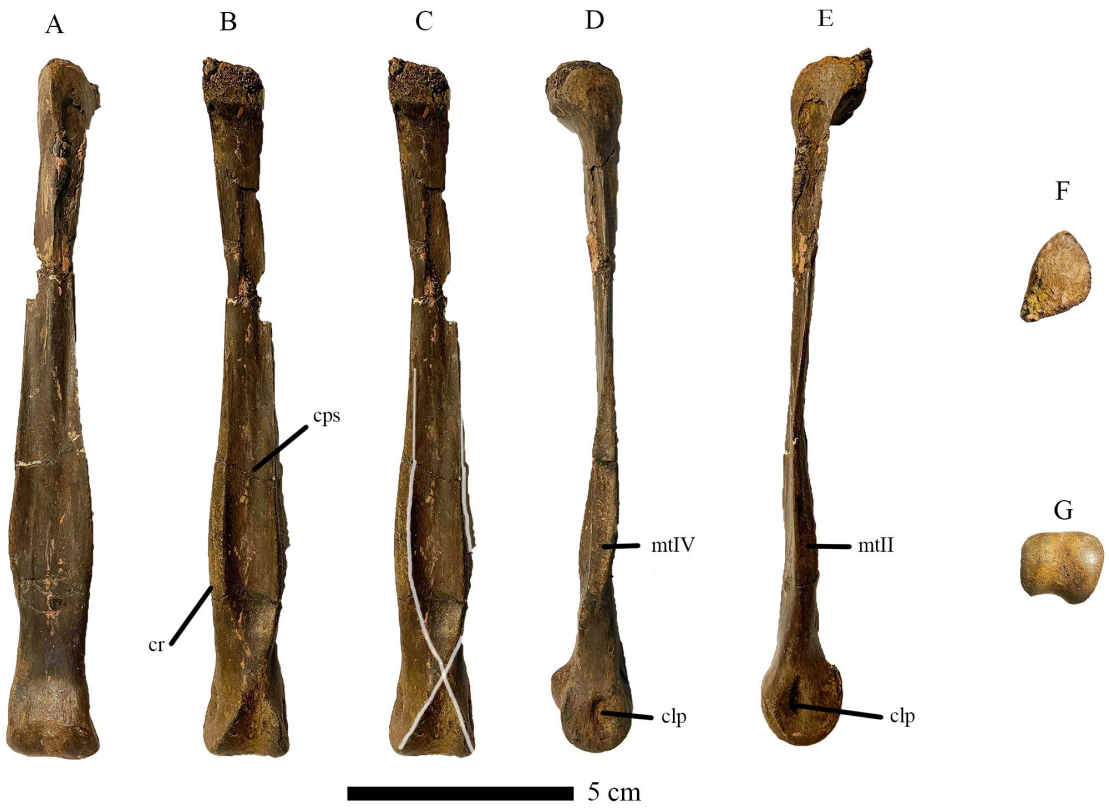

Fig. 3. Right Metatarsal III of CM 96523. Photographs of bone in A) Anterior, B) Posterior, C) Posterior (cruciate ridges highlighted), D) Lateral, E) Medial, F) Proximal, and G) Distal views. Cruciate ridges highlighted in white where visible. Abbreviations: clp, collateral ligament pit; cps, concave posterior surface; cr, cruciate ridges; mtII, articular surface for metatarsal II; mt IV, articular surface for metatarsal IV. Scale bar = 5cm.

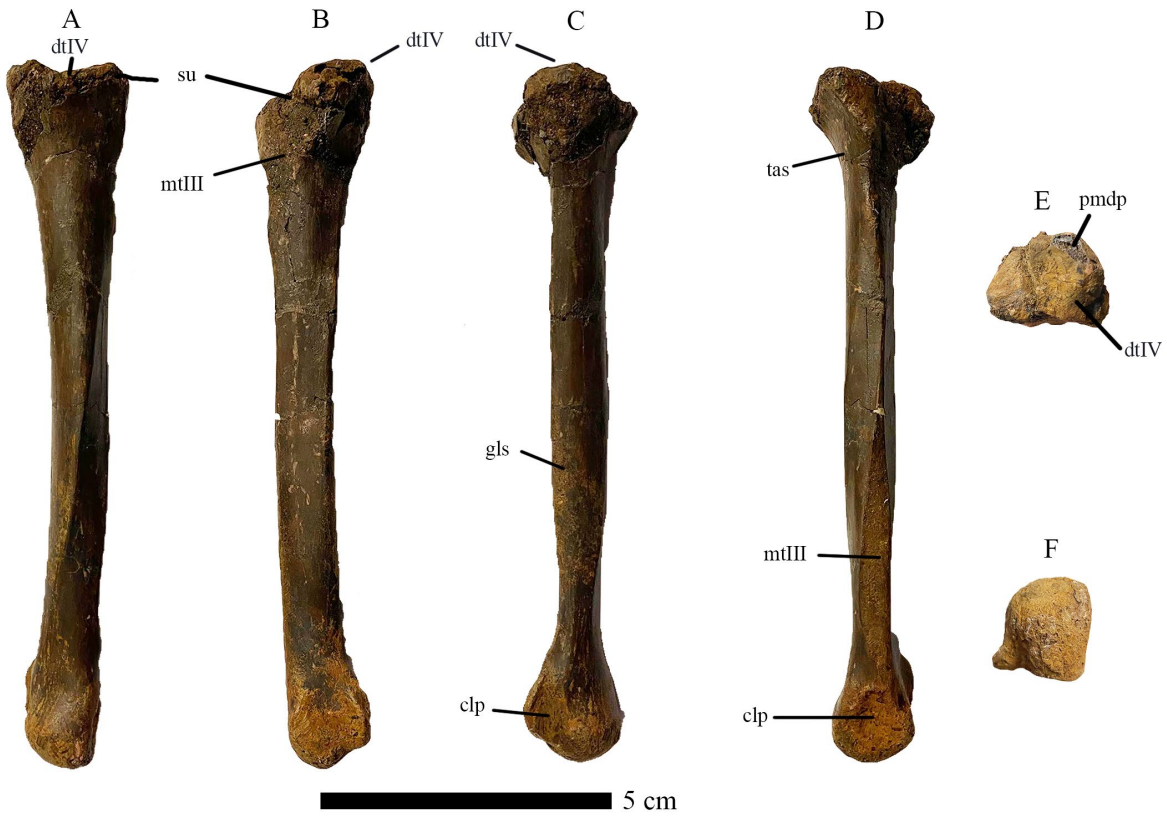

Fig. 4. Right Metatarsal IV of CM 96523. Photographs of bone in A) Anterior, B) Posterior, C) Lateral, D) Medial, E) Proximal, and F) Distal views. Abbreviations: clp, collateral ligament pit; dtIV, distal tarsal IV; gls, M. gastrocnemius pars lateralis insertion scar; mtIII, articular surface for metatarsal III; pmdp, broken base of proximodistal process; su, suture between distal tarsal IV and mt IV; tas, M. tibialis anterior insertion scar. Scale bar = 5cm.

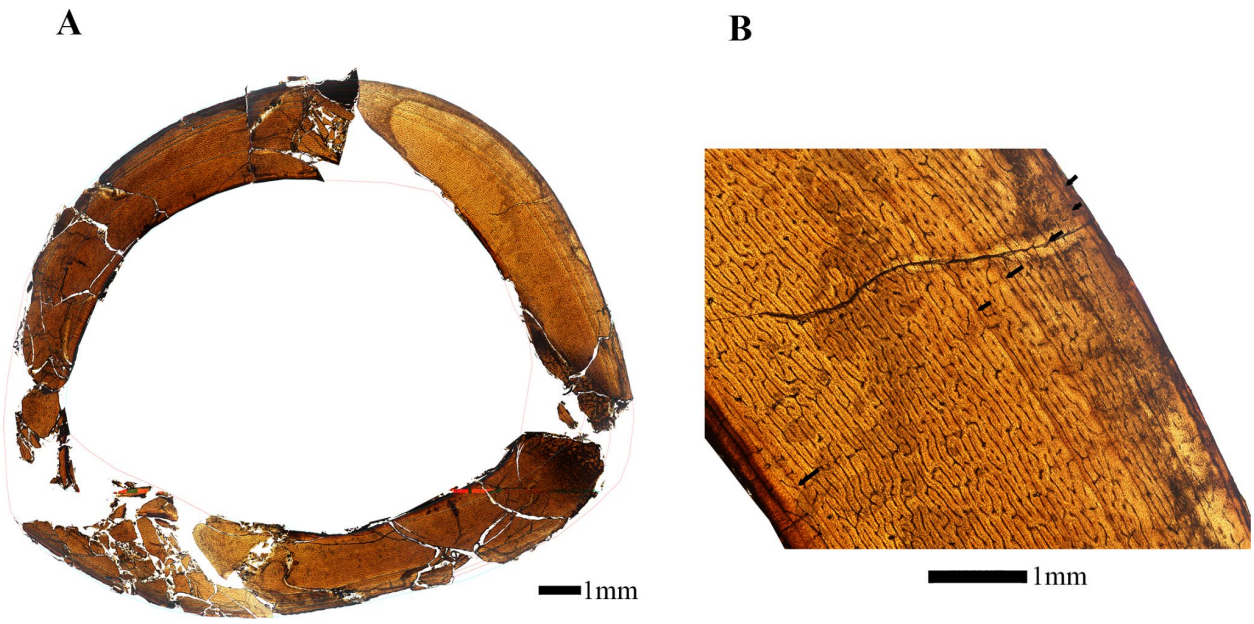

Fig. **5. Osteological thin-section of the femur of CM 96523.** Shown in A) reconstructed circumference, with LAGs highlighted in light blue, and B) close-up with black arrows denoting lines of arrested growth. Note the change in vascularity from inner to outer cortex. Scale bars both equal 1mm.

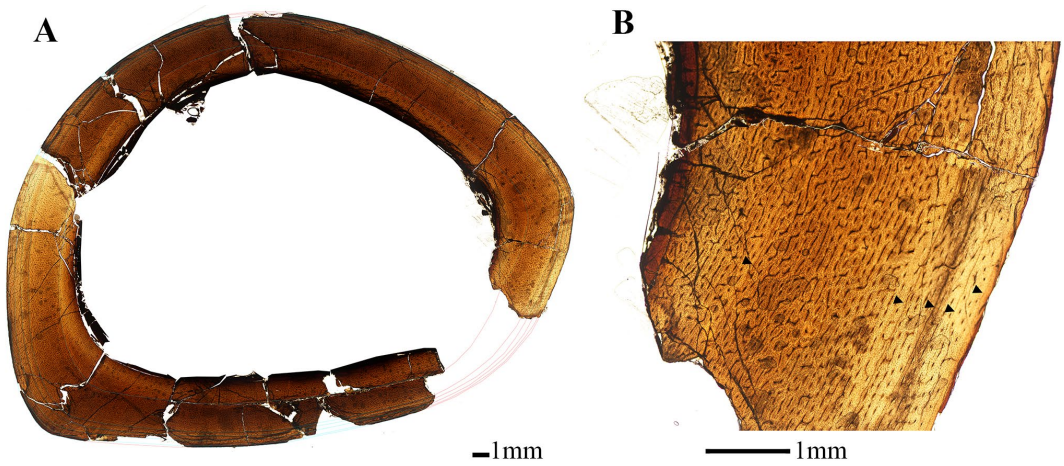

Fig. 6. Cross section of right tibia of CM 96523. Shown in A) reconstructed circumference, with LAGs highlighted in light blue, and B) close-up with black arrows denoting lines of arrested growth. Note the change in vascularity from inner to outer cortex. Scale bars both equal 1mm.

Fig. 7. Cross section of right Metatarsal IV of CM 96523. Shown in A) full section, with LAGs highlighted in light blue, and B) close-up with black arrows denoting lines of arrested growth. Note the change in vascularity from inner to outer cortex. Scale bars both equal 1mm.

Chapter 2

Narrowing the plausible body mass range of the caenagnathid *Anzu wyliei* using volumetric and extant-scaling methods

ABSTRACT

The ability to accurately and reliably estimate body mass of extinct taxa is a vital tool for interpreting the physiology and even behavior of long-dead animals. For this reason, paleontologists have experimented with many possible methods of estimating the body mass of extinct animals, with varying degrees of success. These methods can be divided into two main categories: volumetric mass estimation, and extant scaling methods. Each has advantages and disadvantages, which is why, when possible, it is best to perform both, and compare the results to determine what is best within reason. Here I employ volumetric mass estimation (VME) to calculate an approximate body mass for previously described specimens of *Anzu wyliei* from the Carnegie Museum of Natural History. I also use extant scaling methods to try to obtain a reliable mass estimate for this taxon. In addition, I present the first digital life restoration and convex hull of the dinosaur *Anzu wyliei* used for mass estimation purposes. I found that the volumetric mass estimation using my digital model was 216-280kg, which falls within the range predicted

by extant scaling techniques, while the mass estimate using minimum convex hulls was below the predicted range, between 159-199kg . The VME method for *Anzu wyliei* strongly affirms the predictive utility of extant-based scaling. However, volumetric mass estimates are likely more precise because the models are based on comprehensive specimen anatomy rather than regressions of a phylogenetically comprehensive but disparate sample.

INTRODUCTION

Body mass is an important characteristic of organisms, as it relates to many important life functions such as metabolic rate [1], relative maturity, and biomechanics. However, it is much harder to estimate body mass of extinct taxa, as a variety of factors including taphonomic distortion of bones and the absence of soft tissues obscure much of the necessary information. Paleontologists have developed a wide range of different techniques over the years to try to solve this conundrum, reviewed comprehensively by Brassey et al. (2017) [2] and Campione and Evans (2020) [3]. Currently, mass estimation techniques fall into two major categories - volumetric mass estimates, that use various ways of estimating body volume and density, and extant scaling methods, which use relationships between measured osteological characters and body mass in modern taxa, and attempt to reconcile these relationships with extinct organisms. Each method has advantages and drawbacks, which is why using both at the same time can be informative [3] for identifying potential errors in one method or the other and to provide a more realistic range of values.

I wanted to determine whether volumetric mass estimation could create a narrower range of body mass estimates for a taxon such as *Anzu wyliei* based on known specimens, as well as using more sophisticated extant scaling methods than those used in the original description [4].

Many different methods have been used throughout the years to estimate body mass from volume [5–15]. These have included using a scaled down physical model of the animal of interest [5–7]; more recent techniques include 3D mathematical slicing [9], photogrammetry [8,11,12], and using what are referred to as minimum convex hulls to wrap around a digitized skeletal frame [13,14]. For a thorough review of each of these techniques the reader is referred to Brassey et al. (2017) [2] and Campione and Evans (2020) [3].

Current published mass estimates for *Anzu wyliei* yield a range of 200-300kg [4], based both on femoral circumference [16], and femoral length [17,18]. However, since the original publication of this description, more detailed techniques for estimating body mass using stylopodial circumference have been developed by others that potentially allow for more rigor and further have the added benefit of yielding confidence ranges even for single-point estimates (N. Campione, pers. comm.). Such methods also do not resort to using multiple different techniques of mass estimation. Here, I derive new, updated mass estimates utilizing extant scaling methods developed by Campione et al. (2014) [19] and further refined by Campione and Evans (2020) [3]. I then compare these to volumetric mass estimates obtained by digital scanning of *Anzu* specimens as well as manual digital modeling. Furthermore, I estimated the animal's mass with minimum convex hulling, to see which method yielded a range that was more congruent with that generated from the extant scaling method.

MATERIALS AND METHODS

Volumetric Mass Estimation

To conduct volumetric mass estimation, multiple elements of the paratype specimen (CM 78001) and a second caenagnathid from the Hell Creek Formation, CM 96523 (See Chapter 1) were digitized using photogrammetry. Photos were taken with a Canon EOS Rebel T3i DSLR, and point clouds produced from the photos using Agisoft Metashape. Imperfections in the resulting meshes were corrected manually in ZBrush 2020. To save time and unnecessary corrections for taphonomic distortion, only the more complete and/or better preserved of paired elements was digitized, with the exception of the femur. The elements of CM 78001 digitized using photogrammetry were the left ilium, left pubis, right ischium, both femora, the left tibia, and the right fibula. The elements of the second caenagnathid that were digitized included the left metatarsal III and the right metatarsal IV. While not belonging to *Anzu wyliei*, they were scaled to appropriate proportions using data from a currently unpublished specimen (M. Lamanna, pers. comm. 2020). 3D scans of a series of presacral vertebrae from both CM 78000 and CM 78001 were provided by Lucy Roberts.

To surmount time constraints, the rest of the skeleton was not directly digitized using photogrammetry - instead, the remaining elements were manually sculpted using reference images of preserved elements from anterior, posterior, lateral, dorsal, and ventral perspectives. Manually sculpted elements included cervical and dorsal ribs, sacral and caudal vertebrae and chevrons, the entire pectoral girdle and forelimbs, and the phalanges and unguals of the pes (Fig 1).

An approximate life-restoration of *Anzu wyliei* was first constructed in ZBrush 2020 using the skeletal figures created by Scott Hartman as a starting point, though the tail of the life restoration was straightened to make it easier to match the articulation of the caudal vertebrae once they were digitized. I felt that Scott Hartman's illustrated skeletal reconstruction was a sufficiently accurate starting point as it was used to illustrate the elements of the original specimens in the description of the taxon [4]. The digitized skeleton and air sacs were then placed within this life restoration to mimic the position of the skeleton within the living organism, and corrections were made to fit the skeleton where needed (Fig. 3). These included minor edits to ensure the torso was not too large relative to the ribcage, and the tail matched with the caudal vertebrae.

To calculate volume and subsequently body mass, the model was exported to 3DS Max 2021, where the volume of the entire life model was calculated, as well as the volume of the lungs and air sacs. The lungs and air sacs were finally constructed using knowledge of osteological correlates for air sac intrusion and placement in theropods [20–22], as well as guidance from experts on theropod respiratory systems (S. Gutherz, pers. comm, 2020; Pat O'Connor, pers. comm, 2021) (Fig 2). Since there are no known osteological correlates for thoracic and clavicular air sacs, I decided to do two calculations of body mass. First, I did a calculation using the most conservative model, with only the cervical air sacs, lungs, abdominal air sacs, and trachea present. Second was the more speculative and extensive air sac system (an "Avian model") that included both anterior and posterior thoracic air sacs, and a clavicular air sac, as are present in Avialae (Pat O'Connor, pers. comm, 2021)[20]. In this way I account for the uncertainty in presence or absence of such air sacs, and can determine how it affects our estimate of body mass.

Since the exact body density of extinct organisms is impossible to calculate with certainty, I used two different values for body density to create an upper and lower bound for my model. The lower bound used an estimated density of 800kg/m^3, as has been done for large sauropods in the past, in part because prior researchers assumed that the pneumaticity in their bones would result in an overall lower body density [11], an issue some authors have brought up for highly pneumatic saurischian taxa [3,14,20]. Not all researchers agree on this, however. Increasing skeletal pneumaticity does not appear to change the total mass relative to whole body mass—the skeletons of highly pneumatic birds weigh the same relative to total body mass as less pneumatic birds [23,24]. This could mean that pneumaticity probably does not directly have an effect on whole body density. The negative relationship between density and body mass in birds is probably related to an increase in size of the air sacs relative to total body volume, though at the moment this is simply speculation (S. Gutherz, pers. comm.). To compensate for these possible issues, for the upper bound I used a value of 1000kg/m^3, which many volumetric studies have used when aiming to estimate body mass through volumetric methods [9,10,12,25].

Since previous researchers have used convex hulling methods to estimate body mass of both extant and extinct taxa [13,14], I also used this method for comparative purposes on *Anzu*. To construct minimal convex hulls, first the skeleton was exported from 3DS Max into MeshLab. The skeleton was divided into multiple segments, each given its own convex hull (Fig 4), and each hull was computed for volume. Because correct scaling did not transfer between programs, the Transform: Scale: Normalize function to scale the skeleton as close as possible to the known actual size of the animal was employed. Furthermore, MeshLab's volume output was in cm^3, and thus I converted these volumes to m^3. The total volumes of all of the segments (Table

S1) were summed together, and multiplied by the two extremes of density used for the manually-modeled estimate, to get a range of body masses for comparative purposes.

Extant Scaling Methods

For comparative purposes, I sent data on the femoral circumference of the holotype *Anzu wyliei*, CM 78000, to Dr. Nicolás Campione, to use in his body mass regression analyses as he has done in his previous works [3,19] (Fig 5). We also compared these to the values originally obtained by Lamanna et al. (2014) [4], as using femoral length as an estimator still has its uses, as taphonomic factors can easily distort femoral circumference and make it impossible to accurately measure.

RESULTS

Volumetric Mass Estimation

The volume of the complete life model was 0.30 m^3 (Table 1). The air sac volume differed between the more conservative and the more speculative approach - in the conservative model, the lungs and other pulmonary structures measured a total of 0.02m^3. In the more speculative reconstruction, this volume increased to 0.03m^3. From these results, my conservative model is heavier, at an estimated 224-280kg, while our more speculative model is lighter, ranging from 216-270kg. Minimum convex hulling yielded a volume of 0.199m^3 (Table S1), yielding a mass estimate between 159 and 199kg, depending on which body density value was applied.

Extant Scaling Methods

Because the femoral circumference of CM 78001was not available, I was only able to use the femoral circumference of the holotype *Anzu* specimen, CM 78000, for the extant scaling regression. The resulting regression yielded a body mass range of between 202 and 342kg (Fig 5).

Table 1. Mass Estimates resulting from different methods of estimation.

Note the increasing precision relative to earlier studies provided by the results presented herein. Further note the discrepancy of the minimum convex hull estimate relative to all other estimates.

Source	**Lamanna et al. 2014**	**Nicolás Campione**	**This paper**	**This paper**
Estimation Type	Femoral length	Log stylopodial circumference regression	VME from digitally reconstructed model	VME from minimum convex hulls
Result	200-300kg	202-342kg	216-280kg	159-199kg

DISCUSSION

The results obtained from my volumetric mass estimates of *Anzu wyliei* fit within both the original mass range proposed by Lamanna et al [4] and that predicted by the corroboration plot using Campione's method [19,26]. Thus, my current volumetric mass estimate of 216-280kg

accounting for differing reconstruction of air sacs provides a more precise range of body masses for this organism than those that use extant data alone.

I also found that the minimum convex hulling method seems to lead to an underestimation of total body mass in this case, though this could caused by scaling errors when exporting between programs. However, if this is indeed a reflection upon minimum convex hulling as a method, it appears when comparing the convex hull model to the manually-sculpted life restoration that much of the missing body mass can be accounted for based on the extremely thin volume of both the forelimbs and hindlimbs (Fig. 3, 4). The convex hull model does not account for the *M. iliotbialis, M. iliofibularis*, or many of the other muscles connecting the pelvic bones to the femur, or the *caudofemoralis* muscles on the tail or thigh. The same is true for many of the muscles in the upper arm. This could explain the much lower result and suggests that aspects of the convex hull method may make implausible biological assumptions.

Moreover, it seems likely that with convex hulling, especially on animals with relatively small body volumes (total volume < $1.0m^3$), the choice of which elements to include in a particular convex hull may have a strong influence on the final result. Perhaps if the pelvic bones were included in the same hull as the femur, for example, the resulting hull would have added the muscles to the proximal hindlimb. Yet, even if this change were made, there is still the issue of the incredibly thin zeugopods of both forelimbs and hindlimbs, largely underrepresenting both the *gastrocnemius* muscles and, to a lesser extent, the antebranchial muscles of the forelimb. However, while these areas are clearly given less volume than they would account for in life, both the head, and the autopodia of both forelimbs and hindlimbs account for a greater volume than they would in life. This is again because of the way hulls had to be set up and calculated - since the skull is modeled as a single element despite consisting of an upper and lower jaw (and

the mouth being open in articulation), the hull included the gap between the jaws in its total volume which again is biologically inaccurate. Similarly, since the individual fingers and toes were not added as separate hulls, the generated hull connected them in a single, wide structure, like a duck's foot, which is not correct. Despite these three areas of greater-than-expected volume, they are not sufficient to balance out the underestimation of volume in other regions, resulting in a lower-than-expected body volume regardless of the density value selected.

While the volumetric mass estimate using a manually constructed life restoration has worked well to narrow down a plausible range of body masses for *Anzu wyliei*, I continue to argue for the use of integrated methods making use of both volumetric and extant scaling methods where possible. Volumetric body mass is only possible for taxa known from relatively complete remains [3], which greatly reduces its applicability in the vertebrate fossil record because many taxa are known only from fragmentary material. Furthermore, there are still great unknowns about body density, lung and air sac size and structure, and soft tissue that can also be huge sources of variation within volumetric mass estimates if not carefully accounted for *a priori*. This may be done by creating more than one model, to account for differing amounts of soft tissue as has been implemented by some researchers [25], or as I have done here, simply by using a differing possible body density in the same model. I chose the latter, as the relatively small total volume of the model ($0.30m^3$) and the sensitivity of the software calculating the volume ($\pm 0.01m^3$) meant that it would take the addition or subtraction of an immense amount of extra soft tissue relative to the model size to modify the body mass of the model by more than 10-20kg in either direction (personal obs.). However, with larger taxa, making both maximum and minimum volume models is a more viable approach if using a program with the same sensitivity to volume increases or decreases (ie $\pm 0.01m^3$), while different values for body

density may also be used to add an additional source of variation [3]. Another option I would suggest is to use a lower sensitivity to volume differences, based on the size of the animal being modeled. I cannot say specifically what sensitivities would be optimal for any given taxon, but using this study as a template may prove useful.

CONCLUSIONS

Using carefully sculpted digital models based on known specimens, and using a range of possible body densities, allows for a more realistic and accurate range of possible body masses than extant scaling alone. However, I note that this is only possible when specimens are sufficiently complete and well-known enough to reliably infer basic soft tissue anatomy, and as such extant scaling is still critical for providing a bracket of reasonable values against which to compare those gathered from volumetric methods. Further, I show that there is a great sensitivity of minimum convex hulling to the selection of elements within the hull, making it difficult to determine reliability on creatures wit

REFERENCES

1. Strotz LC, Saupe EE, Kimmig J, Lieberman BS. Metabolic rates, climate and macroevolution: a case study using Neogene molluscs. Proc R Soc B Biol Sci. 2018;285: 20181292. doi:10.1098/rspb.2018.1292
2. Brassey CA, O'Mahoney TG, Chamberlain AT, Sellers WI. A volumetric technique for fossil body mass estimation applied to Australopithecus afarensis. J Hum Evol. 2017;115: 47–64. doi:10.1016/j.jhevol.2017.07.014
3. Campione NE, Evans DC. The accuracy and precision of body mass estimation in non-avian dinosaurs. Biol Rev. 2020;95: 1759–1797. doi:https://doi.org/10.1111/brv.12638
4. Lamanna MC, Sues H-D, Schachner ER, Lyson TR. A new large-bodied oviraptorosaurian theropod dinosaur from the latest Cretaceous of western North America. PLoS One. 2014;9: e92022.
5. Gregory WK. The weight of the *Brontosaurus*. Science. 1905;22: 572–572.

doi:10.1126/science.22.566.572
6. Colbert EH. The weights of dinosaurs. Am Mus Novit. 1962;2076: 1–16.
7. Alexander RM. Mechanics of posture and gait of some large dinosaurs. Zool J Linn Soc. 1985;83: 1–25. doi:10.1111/j.1096-3642.1985.tb00871.x
8. Gunga H-Chr, Kirsch KA, Baartz F, Röcker L, Heinrich W-D, Lisowski W, et al. New data on the dimensions of *Brachiosaurus brancai* and their physiological implications. Naturwissenschaften. 1995;82: 190–192. doi:10.1007/BF01143194
9. Henderson DM. Estimating the masses and centers of mass of extinct animals by 3-D mathematical slicing. Paleobiology. 1999;25: 88–106.
10. Hutchinson JR, Ng-Thow-Hing V, Anderson FC. A 3D interactive method for estimating body segmental parameters in animals: application to the turning and running performance of Tyrannosaurus rex. J Theor Biol. 2007;246: 660–680. doi:10.1016/j.jtbi.2007.01.023
11. Gunga H-C, Suthau T, Bellmann A, Stoinski S, Friedrich A, Trippel T, et al. A new body mass estimation of *Brachiosaurus brancai* Janensch, 1914 mounted and exhibited at the Museum of Natural History (Berlin, Germany). Foss Rec. 2008;11: 33–38. doi:https://doi.org/10.1002/mmng.200700011
12. Bates KT, Manning PL, Hodgetts D, Sellers WI. Estimating mass properties of dinosaurs using laser imaging and 3D computer modelling. PLOS ONE. 2009;4: e4532. doi:10.1371/journal.pone.0004532
13. Sellers WI, Hepworth-Bell J, Falkingham PL, Bates KT, Brassey CA, Egerton VM, et al. Minimum convex hull mass estimations of complete mounted skeletons. Biol Lett. 2012;8: 842–845. doi:10.1098/rsbl.2012.0263
14. Brassey CA, Sellers WI. Scaling of convex hull volume to body mass in modern primates, non-primate mammals and birds. PLOS ONE. 2014;9: e91691. doi:10.1371/journal.pone.0091691
15. Snively E, O'Brien H, Henderson DM, Mallison H, Surring LA, Burns ME, et al. Lower rotational inertia and larger leg muscles indicate more rapid turns in tyrannosaurids than in other large theropods. PeerJ. 2019;7: e6432. doi:10.7717/peerj.6432
16. Anderson JF, Hall-Martin A, Russell DA. Long-bone circumference and weight in mammals, birds and dinosaurs. J Zool. 1985;207: 53–61. doi:https://doi.org/10.1111/j.1469-7998.1985.tb04915.x
17. Christiansen P, Fariña R a. Mass prediction in theropod dinosaurs. Hist Biol. 2004;16: 85–92. doi:10.1080/08912960412331284313
18. Zanno LE, Makovicky PJ. No evidence for directional evolution of body mass in herbivorous theropod dinosaurs. Proc Biol Sci. 2013;280: 1–8.
19. Campione NE, Evans DC, Brown CM, Carrano MT. Body mass estimation in non-avian bipeds using a theoretical conversion to quadruped stylopodial proportions. Methods Ecol Evol. 2014;5: 913–923. doi:https://doi.org/10.1111/2041-210X.12226
20. Benson RBJ, Butler RJ, Carrano MT, O'Connor PM. Air-filled postcranial bones in theropod dinosaurs: physiological implications and the 'reptile'-bird transition. Biol Rev Camb Philos Soc. 2012;87: 168–193. doi:10.1111/j.1469-185X.2011.00190.x
21. Sereno PC, Martinez RN, Wilson JA, Varricchio DJ, Alcober OA, Larsson HCE. Evidence for avian intrathoracic air sacs in a new predatory dinosaur from Argentina. Kemp T, editor. PLoS ONE. 2008;3: e3303. doi:10.1371/journal.pone.0003303
22. Butler RJ, Barrett PM, Gower DJ. Reassessment of the evidence for postcranial skeletal pneumaticity in Triassic archosaurs, and the early evolution of the avian respiratory system. Farke AA, editor. PLoS ONE. 2012;7: e34094. doi:10.1371/journal.pone.0034094
23. Prange HD, Anderson JF, Rahn H. Scaling of skeletal mass to body mass in birds and mammals. Am Nat. 1979;113: 103–122. doi:10.1086/283367
24. Martin-Silverstone E, Vincze O, McCann R, Jonsson CHW, Palmer C, Kaiser G, et al. Exploring the relationship between skeletal mass and total body mass in birds. Mousseau TA,

editor. PLOS ONE. 2015;10: e0141794. doi:10.1371/journal.pone.0141794
25. Hutchinson JR, Bates KT, Molnar J, Allen V, Makovicky PJ. A computational analysis of limb and body dimensions in *Tyrannosaurus rex* with implications for locomotion, ontogeny, and growth. Claessens L, editor. PLoS ONE. 2011;6: e26037. doi:10.1371/journal.pone.0026037
26. Campione NE, Evans DC. A universal scaling relationship between body mass and proximal limb bone dimensions in quadrupedal terrestrial tetrapods. BMC Biol. 2012;10: 60. doi:10.1186/1741-7007-10-60

FIGURES

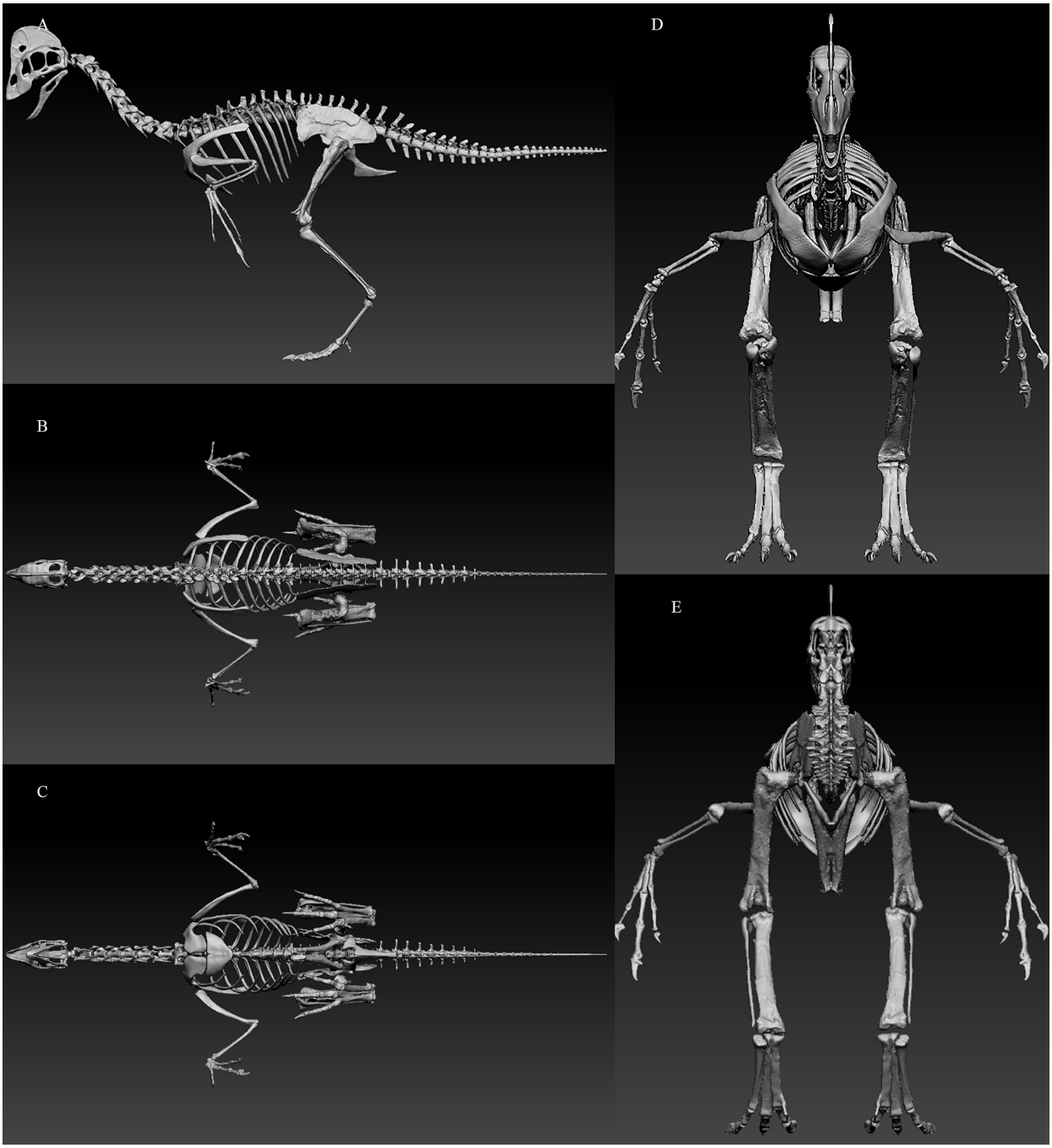

Figure 1. Digitized skeleton of *Anzu wyliei*. Model shown in A) Lateral, B) Dorsal, C) Ventral, D) Anterior, and E) Posterior views.

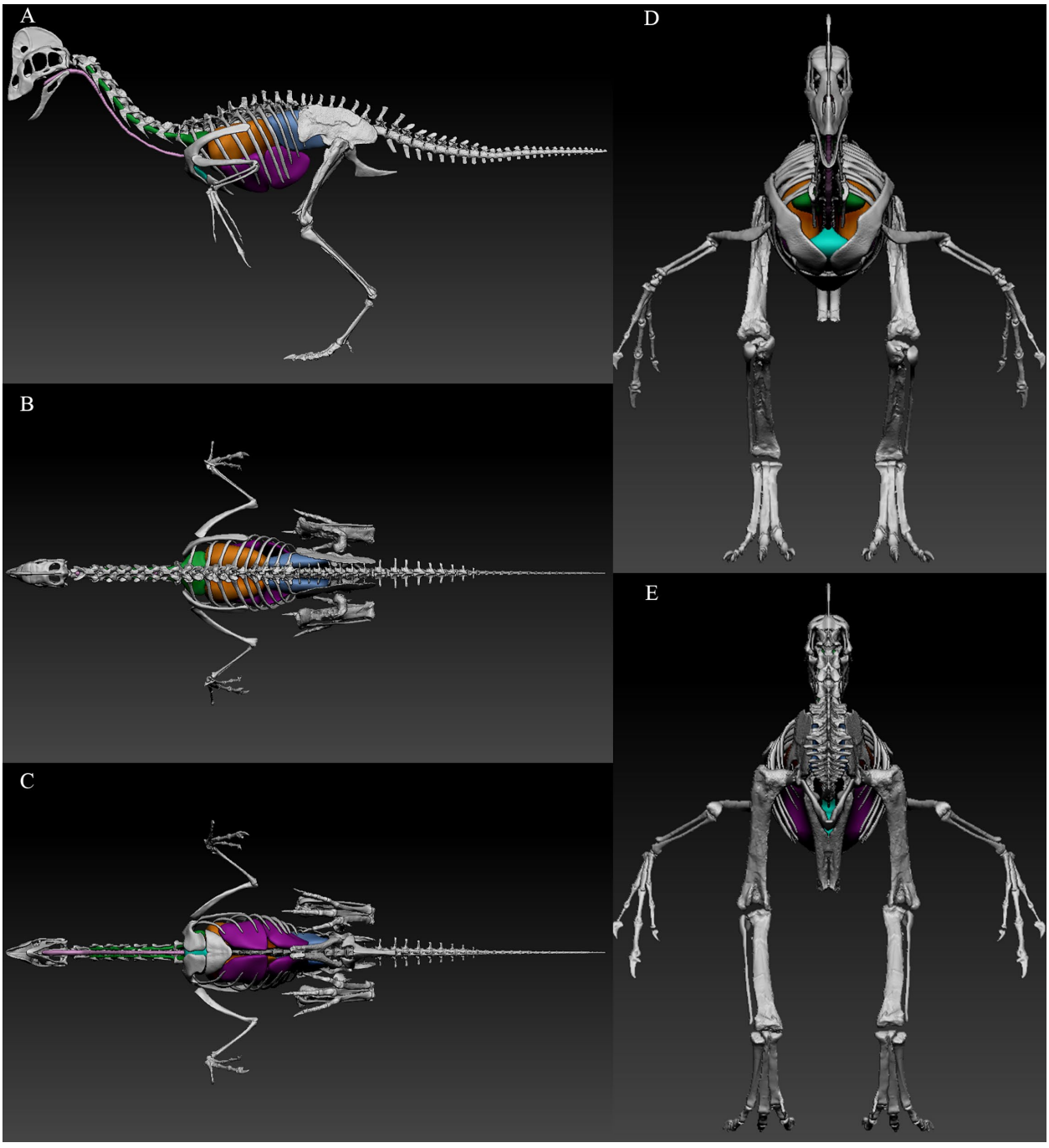

Figure 2. Digitized Skeleton of *Anzu wyliei*, with air sacs ("avian" model). Model shown in A) Lateral, B) Dorsal, C) Ventral, D) Anterior, and E) Posterior views. Key: Green: cervical air sacs; orange: lungs; blue: abdominal air sacs; purple: thoracic air sacs; aquamarine: clavicular air sacs; pink: trachea. NOTE: Clavicular and thoracic air sacs were removed in the more conservative reconstruction.

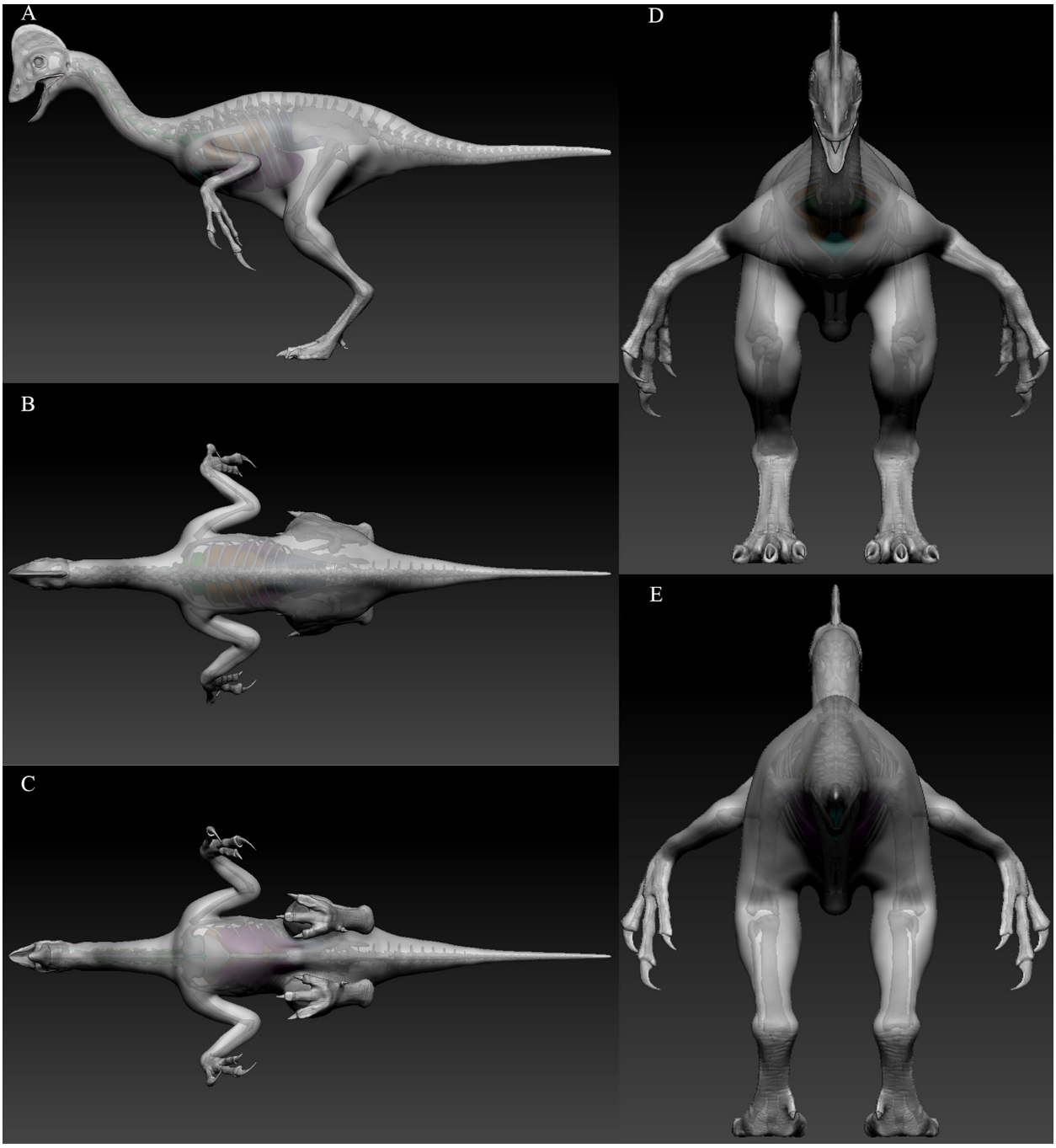

Figure 3. Life restoration of *Anzu wyliei*, with skeleton and air sacs semi-visible through transparency. Model shown in A) Lateral, B) Dorsal, C) Ventral, D) Anterior, and E) Posterior views. Lungs and air sacs as in Figure 2.

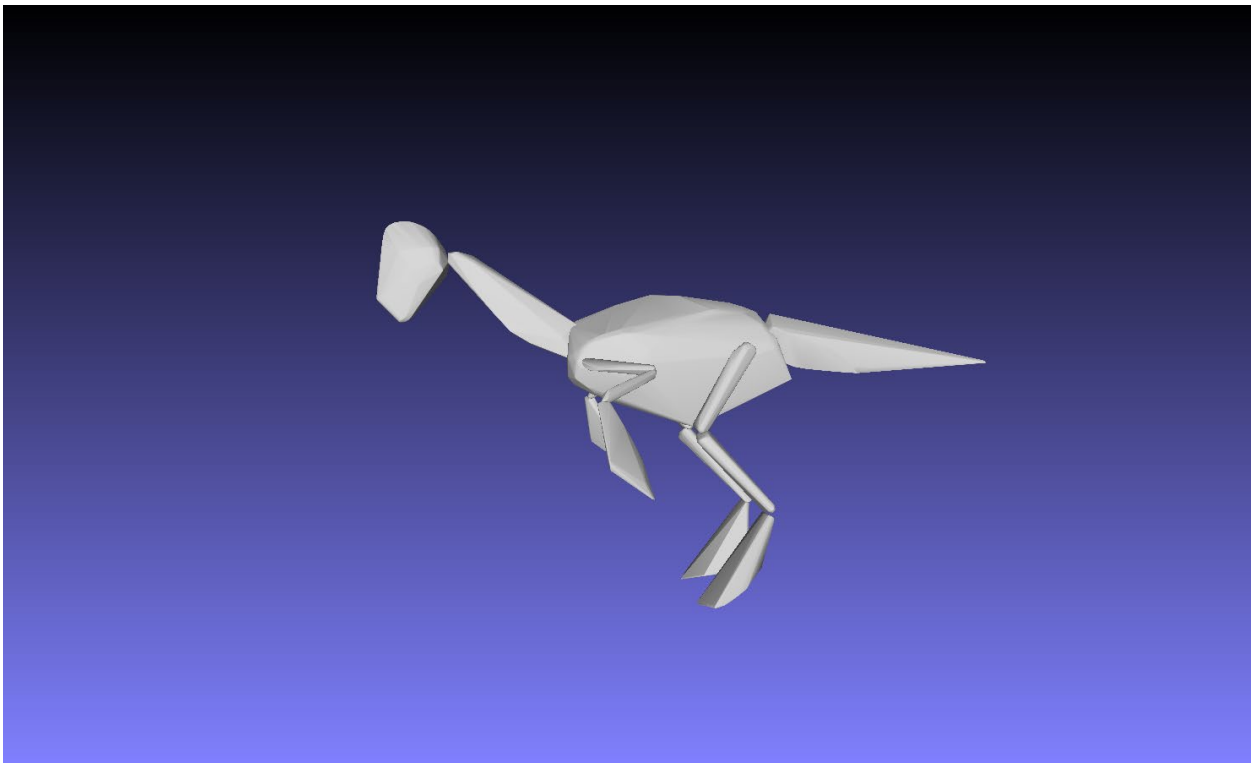

Figure 4. Convex Hull model of *Anzu wyliei*. Depicted in oblique left lateral view.

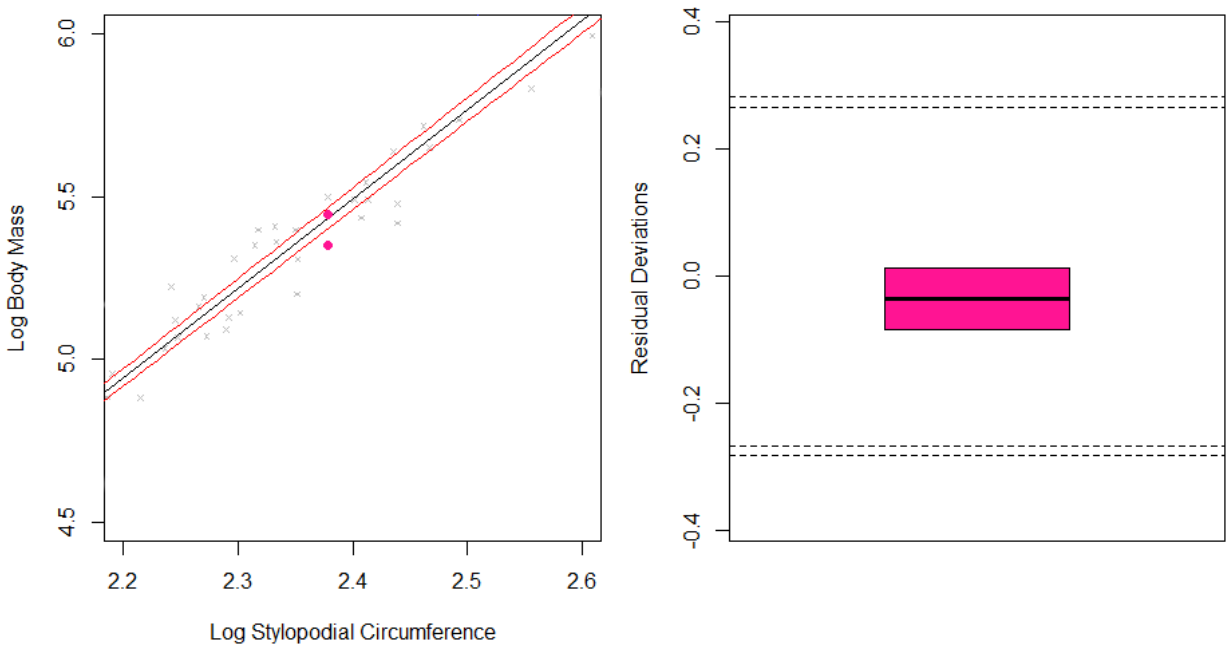

Fig. 5. Logistic regression of stylopodial circumference versus body mass in dinosaurs, and residual deviance. Red lines represent the upper and lower bounds of the 95% confidence interval. The pink dots represent the upper and lower estimates for CM 78000 based on femoral circumference. Gray "x" marks represent other specimens of various taxa used to create the regression. Reproduced with permission from Nicolás Campione.